

Fall 12-20-2019

Cholesterol Biosynthesis in the Nervous System with an Emphasis on Desmosterolosis

Luke Allen
University of Nebraska Medical Center

Follow this and additional works at: <https://digitalcommons.unmc.edu/etd>

 Part of the [Biochemistry Commons](#), [Developmental Neuroscience Commons](#), [Molecular and Cellular Neuroscience Commons](#), and the [Molecular Biology Commons](#)

Recommended Citation

Allen, Luke, "Cholesterol Biosynthesis in the Nervous System with an Emphasis on Desmosterolosis" (2019). *Theses & Dissertations*. 414.
<https://digitalcommons.unmc.edu/etd/414>

This Thesis is brought to you for free and open access by the Graduate Studies at DigitalCommons@UNMC. It has been accepted for inclusion in Theses & Dissertations by an authorized administrator of DigitalCommons@UNMC. For more information, please contact digitalcommons@unmc.edu.

**CHOLESTEROL BIOSYNTHESIS IN THE NERVOUS SYSTEM
WITH AN EMPHASIS ON DESMOSTEROLOSIS**

by

Luke B. Allen

A THESIS

Presented to the Faculty of
the University of Nebraska Graduate College
in Partial Fulfillment of the Requirements
for the Degree of Master of Science

Biochemistry & Molecular Biology Graduate Program

Under the Supervision of Professor Željka Korade

University of Nebraska Medical Center
Omaha, Nebraska

December, 2019

Advisory Committee:

Željka Korade, D.V.M., Ph.D.

Laurey Steinke, Ph.D.

William B. Rizzo, M.D

ACKNOWLEDGEMENTS

I would like to thank Dr. Korade for her instrumental guidance throughout every step of this process and her willingness to take me in to the lab with very little prior experience, especially in the realm of mouse work. I would also like to thank Dr. Karoly Mirnics for always making sure to think of the ‘why?’ as much as the ‘how?’ for any given experiment as well as always keeping the ‘so what?’ in mind. I also thank Dr. Thiago Genaro-Mattos for teaching me essentially everything I know about mass spectrometry and Dana S’Aulis for letting me take over her GC/MS for a week straight. I would also like to thank Dr. Laurey Steinke for her continued support and guidance from the very beginning of my time in the Department of Biochemistry and Molecular Biology. I would also like to thank Dr. William Rizzo and Dr. Melissa Teoh-Fitzgerald for taking time out of their busy schedules in order to serve on my supervisory and exam committees. Finally, I would also like thank the other members of the lab, Allison and Marnie for maintaining the incredibly laid back and collaborative culture our lab has.

CHOLESTEROL BIOSYNTHESIS IN THE NERVOUS SYSTEM WITH AN EMPHASIS ON DESMOSTEROLOSIS

Luke B. Allen, M.S.

University of Nebraska, 2019

Advisor: Željka Korade, D.V.M., Ph.D.

Cholesterol biosynthesis is integral to proper neurodevelopment due to the reliance on *de novo* synthesis of cholesterol in the brain. Disruptions in this process have devastating outcomes for human life characterized by several phenotypic manifestations concomitant with developmental delay. The cholesterol biosynthesis disorder desmosterolosis is an extremely rare disorder with a severe clinical phenotype, however, the models used to study this disease are not well characterized. In addition to genetic disruptions in cholesterol biosynthesis, pharmacological perturbation is an understudied side effect of many commonly prescribed drugs. Here we present a characterization of the sterol profile of the mouse model of desmosterolosis followed by an examination of one such pharmacological inhibitor of cholesterol biosynthesis, amiodarone. Amiodarone is a commonly prescribed medication used to treat life-threatening atrial and ventricular arrhythmias with the primary target being potassium channels and beta adrenergic receptors. We show that amiodarone is also a potent inhibitor of several cholesterol biosynthesis enzymes in various cell culture models, affecting the enzymes 24-dehydrocholesterol reductase (Dhcr24) and emopamil binding protein (Ebp). Additionally we show that the serum of amiodarone users have elevated levels of desmosterol, zymosterol, zymostenol and 8-dehydrocholesterol. Our study provides evidence that the use of various medications, unrelated to cholesterol metabolism, may lead to potentially severe clinical consequences related to the inhibition of sterol biosynthetic enzymes.

TABLE OF CONTENTS

Acknowledgements -----	i
Table of Contents -----	iii
List of Figures -----	v
list of tables -----	vi
List of Abbreviations -----	vii
Chapter 1: Introduction -----	1
Cholesterol biosynthesis -----	1
Cholesterol: an essential biomolecule for neurodevelopment -----	1
Cholesterol biosynthesis disorders -----	3
Desmosterolosis -----	5
History of desmosterolosis mouse models -----	6
Pharmacological inhibition of Dhcr7 and Dhcr24 -----	8
Effects of amiodarone on cholesterol biosynthesis -----	10
Chapter 2: Methods -----	12
Mouse studies -----	12
Study population -----	12
Primary neuronal cultures -----	13
Primary astrocytic cultures -----	13
Control Neuro2a and <i>Ebp</i> -deficient Neuro2a cultures -----	14
Immunocytochemistry and imaging -----	14
RNA isolation and clean-up -----	15
Complementary DNA synthesis and RT ² Profiler PCR Mouse Arrays -----	15
Western blotting -----	15
Cell counting -----	16
Sterol extraction for HPLC-MS/MS analysis -----	16
HPLC-MS/MS (SRM) analyses of sterols -----	17
Sterol extraction for GC-MS analysis of sterols -----	18
GC-MS analysis of sterols -----	18
Serum drug extraction -----	19
Serum drug measurements -----	19
Statistical analyses -----	19
Chapter 3: Results -----	21
Cholesterol, desmosterol and 7-DHC levels show a developmental trajectory -----	21

Cholesterol deficiency leads to early postnatal death -----	22
Desmosterol is greatly elevated in the brains of <i>Dhcr24</i> -deficient mice -----	23
Desmosterol is elevated in <i>Dhcr24</i> -Het mice compared to WT littermates-----	23
Elevated desmosterol levels result in complex transcriptional changes -----	25
High desmosterol levels alter neuronal outgrowth-----	27
Amiodarone affects post-lanosterol cholesterol biosynthesis in neuronal and glial cells -----	29
Amiodarone inhibits the sterol biosynthetic enzyme EBP -----	30
Amiodarone users have elevated serum levels of desmosterol, 8-DHC, zymosterol and zymostenol-----	33
Chapter 4: Discussion-----	36
Role of desmosterol in neuronal development-----	36
Amiodarone affects cholesterol biosynthesis -----	39
Conclusions-----	43
Appendix A: Sterol information -----	46
Appendix B: Sterol biosynthesis disorders -----	46
Appendix C: Network statistics of altered transcripts from PCR arrays -----	47
Appendix D: Zymosterol and zymostenol GC-MS chromatograms and mass spectra-----	48
Appendix E: Reagent table-----	49
Bibliography-----	50

LIST OF FIGURES

Figure 1: Cholesterol biosynthesis scheme. -----	2
Figure 2: Chemical structure of amiodarone (CAS 1951-25-3) and triparanol (metasqualene; CAS 78-41-1).-----	10
Figure 3: Ontogeny of cholesterol, desmosterol and 7-DHC in the mouse brain from E9 to P240. -----	21
Figure 4: Knockout of <i>Dhcr24</i> affects viability and birth weight of mice. -----	22
Figure 5: Desmosterol is greatly elevated in the brains of <i>Dhcr24</i> -deficient mice. -----	23
Figure 6: Cholesterol and desmosterol levels are not affected by maternal genotype. -----	24
Figure 7: Desmosterol levels are greatly elevated in nervous tissue of <i>Dhcr24</i> -Het mice. -----	25
Figure 8: Interaction network of altered transcripts from PCR arrays.-----	28
Figure 9: MAP2 expression is elevated in <i>Dhcr24</i> -KO brain. -----	29
Figure 10: Amiodarone elevates zymosterol and zymostenol in cells.-----	31
Figure 11: Comparison of genetic and chemical inhibition of EBP. -----	32
Figure 12: Amiodarone and MDEA are present in patient serum. -----	34
Figure 13: Sterol measurements in human serum samples. -----	35
Figure 14: Sterol measurements in human serum samples that received oral administration of amiodarone.-----	41
Figure 15: Network statistics of altered transcripts from PCR arrays. -----	47
Figure 16: GC-MS analysis of zymosterol.-----	48
Figure 17: GC-MS analysis of zymostenol. -----	48

LIST OF TABLES

Table 1: Elevated desmosterol changes lipoprotein signaling, cholesterol biosynthesis transcripts, synaptic plasticity transcripts, nuclear receptors and coregulators. -----	27
Table 2: Common names of sterols used with detailed information. -----	46
Table 3: Comparison of cholesterol synthesis disorders. -----	46

LIST OF ABBREVIATIONS

7-DHC	7-Dehydrocholesterol
7-DHD	7-Dehydrodesmosterol
8-DHC	8-Dehydrocholesterol
ANOVA	Analysis of variance
APCI	Atmospheric pressure chemical ionization
ASD	Autism spectrum disorder
BCA	Bicinchoninic acid
BEH	Ethylene bridged hybrid
BHT	Butylated hydroxytoluene
Bis-Tris	Bis(2-hydroxyethyl)amino-tris(hydroxymethyl)methane
BSTFA	N,O-Bis(trimethylsilyl)trifluoroacetamide
cDNA	Complementary deoxyribonucleic acid
CDPX2	Chondrodysplasia punctate 2 X-linked
Chol	Cholesterol
CNS	Central nervous system
CoA	Coenzyme A
<i>Dhcr24</i>	24-Dehydrocholesterol reductase
<i>Dhcr7</i>	7-Dehydrocholesterol reductase
DMSO	Dimethyl sulfoxide
DNase	Deoxyribonuclease

E15	Embryonic day 15
EDTA	Ethylenediaminetetraacetic acid
EIC	Extracted ion chromatogram
FBS	Fetal bovine serum
GAPDH	Glyceraldehyde 3-phosphate dehydrogenase
GC-MS	Gas chromatography mass spectrometry
HBSS	Hanks' balanced salt solution
Het	Heterozygous
HMGCR	3-hydroxy-3-methylglutaryl-coenzyme A reductase
HPLC-MS/MS	High-performance liquid chromatography-tandem mass spectrometry
KO	Knock-out
MAP2	Microtubule associated protein 2
MDEA	Mono-N-desethylamiodarone
min	Minutes
NPC	Niemann-Pick type C disease
P0	Postnatal day 0
PCR	Polymerase chain reaction
PTAD	4-Phenyl-1,2,4-triazoline-3,5-dione
PVDF	Polyvinylidene difluoride
qPCR	Quantitative polymerase chain reaction
RCF	Relative centrifugal force

RIPA	Radioimmunoprecipitation assay
RNA	Ribonucleic acid
RT	Room temperature
SDS	Sodium dodecyl sulfate
SEM	Standard error of the mean
SLOS	Smith-Lemli-Opitz syndrome
SRM	Selected reaction monitoring
TBS	Tris-buffered saline
TIFF	Tagged image file format
TPP	Triphenylphosphine
Tris	Tris(hydroxymethyl)aminomethane
UNMC	University of Nebraska Medical Center
UPLC	Ultra-performance liquid chromatography
v/v	Percent by volume
WT	Wild type

CHAPTER 1: INTRODUCTION

Cholesterol biosynthesis

About 20-25% of cholesterol biosynthesis occurs in the liver, with additional synthesis taking place in the brain, intestines, adrenal glands, and reproductive organs [1-4]. Cholesterol is synthesized from acetyl-CoA through many, enzymatically processed intermediates (**Figure 1**) [5]. Cholesterol biosynthesis can be broken down into two major segments: pre-squalene and post-squalene cholesterol synthesis. Post-squalene synthesis converts lanosterol to cholesterol through two major synthetic pathways: the Kandutsch-Russell pathway (favored in most tissues) and the Bloch pathway. The Kandutsch-Russell pathway proceeds through a complex series of reactions (lanosterol through zymostenol and lathosterol ending in 7-dehydrocholesterol (7-DHC)), meanwhile the parallel Bloch pathway proceeds from lanosterol through zymosterol to desmosterol [6]. The conversion of 7-DHC to cholesterol by DHCR7 and the conversion of desmosterol to cholesterol by DHCR24 are the last steps in cholesterol biosynthesis [7, 8].

Cholesterol: an essential biomolecule for neurodevelopment

While the brain accounts for only 2% of total body weight in humans, it contains about 25% of all lipids. Cholesterol accounts for 20-30% of all lipids in the brain [6, 9, 10]. Cholesterol metabolism in the brain differs markedly from that of other tissues due to the blood brain barrier preventing cholesterol uptake from the circulation, thus the brain relies fully on *de novo* cholesterol synthesis [11]. Importantly, cholesterol is synthesized by neurons: HMGCR and DHCR7, the first and last enzymes in the cholesterol biosynthesis pathway, are strongly co-expressed at high levels in neurons throughout the adult murine brain [12]. The function of cholesterol in the central nervous system (CNS) goes beyond being a structural component of cellular membranes and lipid rafts: it is required for synapse and dendrite formation, axonal guidance, and serves as a precursor for various biosynthetic pathways [13]. Furthermore, it plays a critical role in the activity of the sonic hedgehog pathway, an important signaling cascade that regulates morphogenesis in the brain [14].

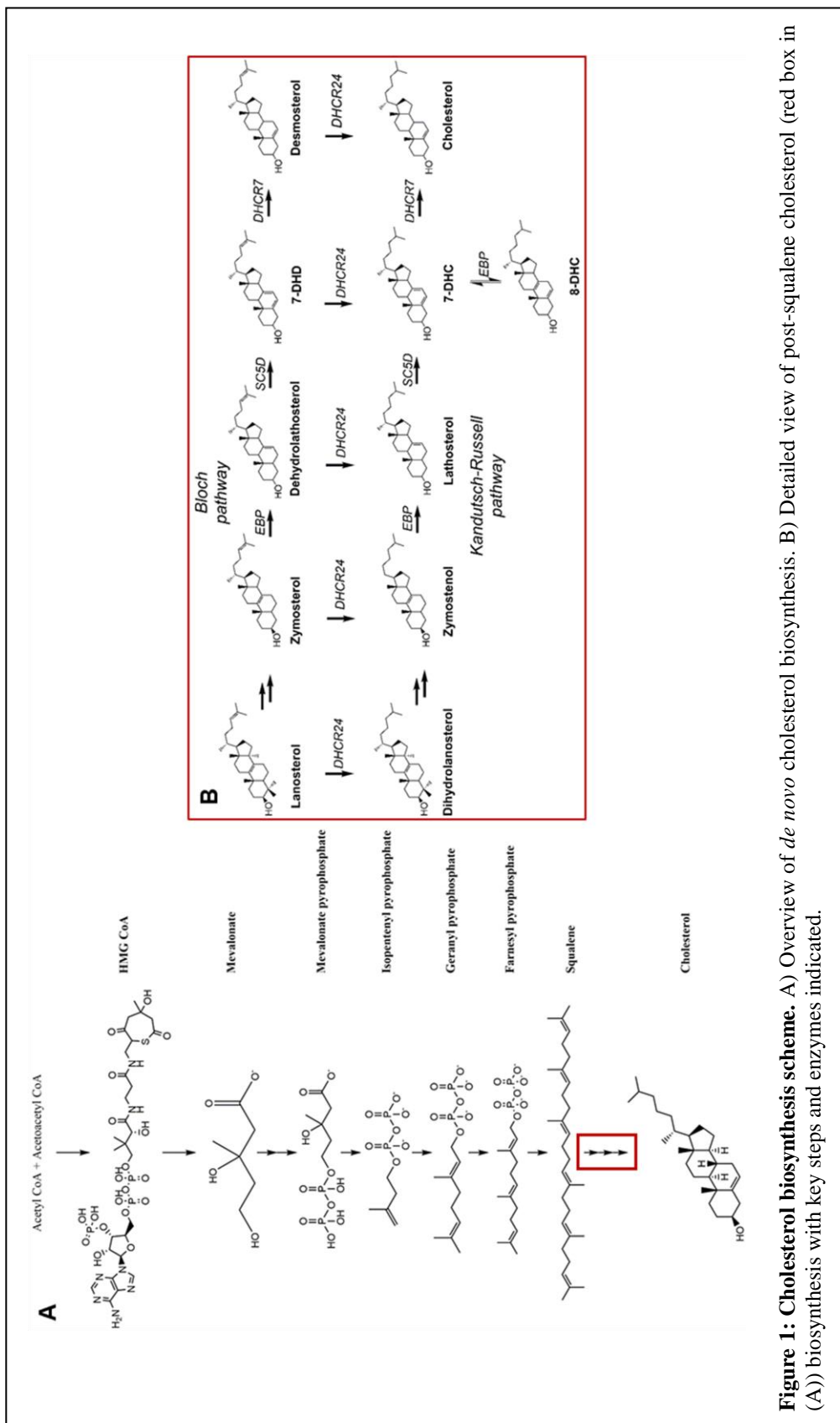


Figure 1: Cholesterol biosynthesis scheme. A) Overview of *de novo* cholesterol biosynthesis. B) Detailed view of post-squalene cholesterol (red box in (A)) biosynthesis with key steps and enzymes indicated.

While endogenous cholesterol synthesis is essential for proper brain development, intact

cholesterol metabolism is also critical for normal function of the adult brain: in the elderly, high circulating cholesterol is associated with better memory function and conversely, low serum cholesterol is associated with an increased risk for depression [15, 16]. Dysfunction of the cholesterol biosynthesis pathways and/or metabolism leads and contributes to a number of neurodevelopmental and neurodegenerative disorders such as Smith-Lemli-Opitz Syndrome (SLOS) [17, 18], desmosterolosis [19-26], Niemann-Pick type C (NPC) disease [27], Huntington's disease [28-32], and Alzheimer's disease [28, 32].

Cholesterol biosynthesis disorders

Defects in cholesterol biosynthesis present with severe abnormalities and developmental disability [21, 22, 33-37]. In the post-lanosterol portion of the pathway there are several disorders described, with the most prevalent being SLOS. Other disorders described in the literature include lathosterolosis, X-linked dominant chondrodysplasia punctata 2 (CDPX2) and desmosterolosis. With the exception of CDPX2, all sterol biosynthesis disorders discussed hereinafter follow an autosomal recessive inheritance pattern. First we will discuss SLOS, the most common post-lanosterol cholesterol biosynthesis disorder, followed by lathosterolosis, which presents with a very similar clinical phenotype to SLOS, followed by CDPX2 and finally desmosterolosis, on which a majority of the following work focuses on.

SLOS is caused by mutations in both copies in the gene encoding the last enzyme in the cholesterol biosynthesis pathway – 7-dehydrocholesterol reductase (*DHCR7*) [38]. These can be either identical (homozygous) or different on each allele (compound mutations) [39-41], one inherited from each parent. It has a prevalence of ~1: 20,000 births, with males and females equally affected [10, 42]. It is believed that heterozygous *DHCR7* mutation carriers have >1% frequency in the human population (9, 27, 32). To date, more than 165 *DHCR7* missense mutations have been identified, and when the two loss or reduced function mutant alleles combine, they result in SLOS with varying degrees of clinical severity, depending on how much *DHCR7* function is retained [41, 43]. Mutations that completely abolish cholesterol biosynthesis are incompatible with life,

therefore only mutations that spare at least some cholesterol biosynthesis are observed. Mutations in *DHCR7* result in diminished cholesterol and desmosterol biosynthesis and accumulation of the precursor 7-DHC in various tissues [17]. SLOS is characterized by multiple congenital malformations and defects, photosensitivity, impaired cognitive function, and behaviors of autism spectrum disorder (ASD) [44, 45].

Lathosterolosis was first described in 2002 in an infant presenting with severe congenital microcephaly, hexadactyly of the left foot, syndactyly of multiple toes and liver dysfunction detected in the first year of life. During the first two years, severe psychomotor delays became apparent, with the deficits closely resembling the SLOS phenotype. However, biochemical analysis revealed a lack of 7-DHC accumulation which is the biochemical hallmark of SLOS. Instead, this patient had greatly elevated levels of lathosterol and upon further investigation it was revealed that fibroblasts from this patient had impaired SC5D activity. To date, there have been only 5 cases of lathosterolosis reported in humans, with the most recent case being very mild and diagnosed much later in life than the four previous cases [46]. Due to the phenotypic overlap of SLOS and lathosterolosis the first four reported cases of lathosterolosis required exclusion of SLOS by way of sterol profiling to arrive at the diagnosis of lathosterolosis.

CDPX2 arises from mutations in the emopamil binding protein (*EBP*) gene which encodes for the cholesterol biosynthetic enzyme sterol-delta(8)-isomerase. CDPX2 patients present with skin defects as well as skeletal abnormalities including short stature and craniofacial defects [47]. Biochemically, patients present with elevated levels of 8-dehydrocholesterol (8-DHC) and zymostenol [48]. The ‘Tattered’ mouse model contains a semi-dominant mutation in the *Ebp* gene that is prenatally lethal for males while females survive but are smaller in stature and have coat striping similar to the skin phenotype of heterozygous human females with CDPX2. The striping of the mouse coat and the analogous skin defects in humans such as whorled atrophic and pigmentary lesions, striated hyperkeratosis, coarse lusterless hair and alopecia as well as the

craniofacial defects present in both Tattered mice and humans have been linked to alterations in the function of EBP. Due to the X-linked nature of the disease, very few cases have been reported in males as CDPX2 is typically lethal in males which is recapitulated in the Tattered mice [49]. One report of a male with CDPX2 attributed survival to his 47,XXY karyotype, while other reports of males with CDPX2 attribute survival to hypomorphic mutations or single gene mosaicism [50-52]. The characteristic features of epiphyseal and periepiphyseal stippling, asymmetries, patchy alopecia of the scalp, brow, and lashes, linear arrays of hypotrophic changes of the skin, structural vertebral anomalies and scoliosis, characteristic facial features, polydactyly and small stature have been observed in both female and male patients with CDPX2, though not all features are present in every patient.

Desmosterolosis

Desmosterolosis is a rare autosomal recessive disorder caused by mutations in the *Dhcr24* gene that encodes the enzyme 24-dehydrocholesterol reductase. Homozygous or heterozygous *Dhcr24* mutations result in systemic elevation of desmosterol and decreased levels of total cholesterol [20, 22, 26]. The *Dhcr24* gene is mapped to chromosome 1p33-p31.1 and eight missense mutations have been described in the coding region of 1550 bp (NM_014762.3) to date. Observed clinical findings of desmosterolosis include shortening and flexion of extremities, brain malformations such as hydrocephalus, absent septum pellucidum and thin corpus callosum, dysmorphic facial features, syndactyly, developmental delay and diaphragmatic eventration [20-22, 24-26].

Desmosterolosis and SLOS have overlapping clinical findings and mouse models of both disorders lead to early postnatal death [19]. It seems that the accumulation of desmosterol is more detrimental than the accumulation of 7-DHC, as *DHCR24* mutations in humans are most often incompatible with life – there are only 10 reported cases of desmosterolosis in the literature since the first report in 1998 [23]. The number of reported cases of desmosterolosis is likely to increase as diagnostic tools available to clinicians advance and genetic sequencing of newborns becomes

more common. Given our experience in characterizing the SLOS mouse model, we decided to undertake the characterization of the mouse model of desmosterolosis as well. The analysis of the desmosterolosis model and comparison to the SLOS model help to illustrate the importance of desmosterol and 7-DHC in neuronal development in addition to the consequences lack of cholesterol has on this process.

History of desmosterolosis mouse models

The original *Dhcr24* knockout mice (C57BL/6x129SvEv) were described by the laboratory of Dr. Elena Feinstein (mice were generated through service agreement with Lexicon Genetics Incorporated). The targeting vector had a 249 bp deletion in *Dhcr24* exon 1 and was electroporated into 129/SvEv^{Brd} (Lex-1) ES cells. The ES cell clones were microinjected into C57BL/6 albino blastocysts and the resulting chimeras were mated to C57BL/6 (albino) females to generate mice heterozygous for the *Dhcr24* mutation. There are three articles published by the senior team of Drs. E. Feinstein and I. Bjorkhem. The first report is in Science 2003 [53], the second in JBC 2006 [54] and the third in Arterioscler Thromb Vasc Biol 2007 [55]. The Science 2003 is a one-page report, with one figure and two supplemental figures showing that *Dhcr24*-KO mice are viable and survive [53]. The JBC 2006 manuscript used these same mice and analyzed CYP46A1 transcriptional regulation [54]. In Figure 2A of the 2006 JBC manuscript there is a graph showing brain cholesterol and desmosterol concentration in WT and *Dhcr24*-KO mice but these data were recalculated from the Science 2003 article. The ATVB 2007 manuscript [55] studies the same mouse model by the same investigators, comparing *Dhcr24*-KO mice with *Dhcr24*-Het mice however, there is no data presented for WT mice. The focus of study was the hepatic sterol homeostasis which included the analysis of hepatic mRNA levels for sterol related genes, bile acids quantification and measurements of plasma oxysterols [55].

In the meantime, the original *Dhcr24* knockout mice were made available to other investigators who initiated backcrossing of *Dhcr24*-KO mice to C57BL/6J background. In addition to the initial three reports [53-55], there were four more publications from the Seo group [56-59]

and one publication by Kuehnle et al. [60] using *Dhcr24*-KO mice. The Seo group (Nagoya University, Japan) obtained mice from Quark Biotech Inc. (Fremont, CA) and backcrossed with C57BL/6J for more than five generations and described the phenotype [58] that is identical to phenotype described in the current study. Three publications by this group focused on skin changes in *Dhcr24*-KO mice [57-59] and one was focused on mouse embryonic fibroblasts isolated from *Dhcr24*-KO mice [56]. Kuehnle et al. obtained mice from Quark [60] performing experiments in SH-SY5Y cells and in primary neuronal cultures from WT and *Dhcr24*-KO brains, but provided no details on the mouse phenotype. This group cultured primary neurons in presence of serum and cholesterol. Based on our experience with primary neuronal cultures (and various cellular models of SLOS), the phenotype (elevated desmosterol) does not manifest in the presence of serum and cholesterol. Thus, we grow cortical neurons in serum-free defined medium without cholesterol supplementation as described in Chapter 2: Primary neuronal cultures.

Information available from the Jackson Laboratory website (<https://www.jax.org/strain/012564>; under the tab Details>Development) states the following: “This same mouse model developed by Dr. Feinstein’s group was sent to Dr. Shailendra B. Patel (while at Medical University of South Carolina) where they were backcrossed to C57BL/6J mice for three generations. Dr. Patel moved his colony to Medical College of Wisconsin, and then further backcrossed the colony to C57BL/6J mice for 11 more generations. Heterozygous mice backcrossed to C57BL/6J for total of at least 14 generations were sent to The Jackson Laboratory Repository. Upon arrival, mice were bred to C57BL/6J (Stock No. 000664) for at least one generation to establish the colony.” We purchased these mice from the Jackson Laboratory.

Compared to the original Science 2003 [53] report that *Dhcr24*-KO mice are viable, these same mice on C57BL/6J background are neonatal lethal. The *Dhcr24*-KO phenotype (reduced number of *Dhcr24*-KO pups at birth; if born, lethal shortly after birth; wrinkle-free skin) has been

reproduced by the investigators in Japan and now by us. While Seo's group focused on the role of Dhcr24 in the skin, we present data relevant to central nervous system development.

Pharmacological inhibition of Dhcr7 and Dhcr24

While essential for life as an integral part of membranes and indispensable for the nervous system, cholesterol has a bad reputation as the culprit in hypertension and cardiovascular diseases [61]. Therefore over the last seven decades pharmaceutical companies have worked to develop compounds to inhibit cholesterol synthesis. Initial efforts focused on the inhibition of the last two enzymes in the pathway, Dhcr7 and Dhcr24. In 1960 the drug triparanol (BIBX79, NB-598, MER-29) was introduced in the US as the first synthetic cholesterol-lowering drug. However, due to severe adverse effects the drug was withdrawn in 1962 [62]. Triparanol decreased cholesterol levels by inhibiting Dhcr24 while simultaneously elevating desmosterol levels.

Another sterol synthesis inhibitor, AY9944, was found to be teratogenic [63] before entering into clinical trials. This compound is an inhibitor of Dhcr7 and is currently used to induce a pharmacological model of Smith-Lemli-Opitz syndrome in rats [64]. Pregnant rats are injected with AY9944 and the injections continue in newborn pups until they reach 3 months of age. AY9944 is very toxic, so much so that very low concentrations of the drug have to be injected to prevent lethal phenotype. The AY9944-treated rats have biochemical profiles characteristic for SLOS and develop retinal degeneration [65].

Another example of chemical inhibition of Dhcr7 with negative consequences is the use of the frequently prescribed antipsychotic, aripiprazole. Cell culture studies have shown that aripiprazole inhibits the Dhcr7 enzyme [66-68]. Analysis of samples from patients taking aripiprazole showed that 7-DHC is significantly elevated in their blood [69]. Studies in our laboratory have shown that, when given to pregnant mice, aripiprazole increases 7-DHC in progeny in both tissue and serum. This biochemical change, greatly elevated 7-DHC, is a characteristic finding present in tissues and serum of the mouse model of SLOS [70]. Aripiprazole is not currently

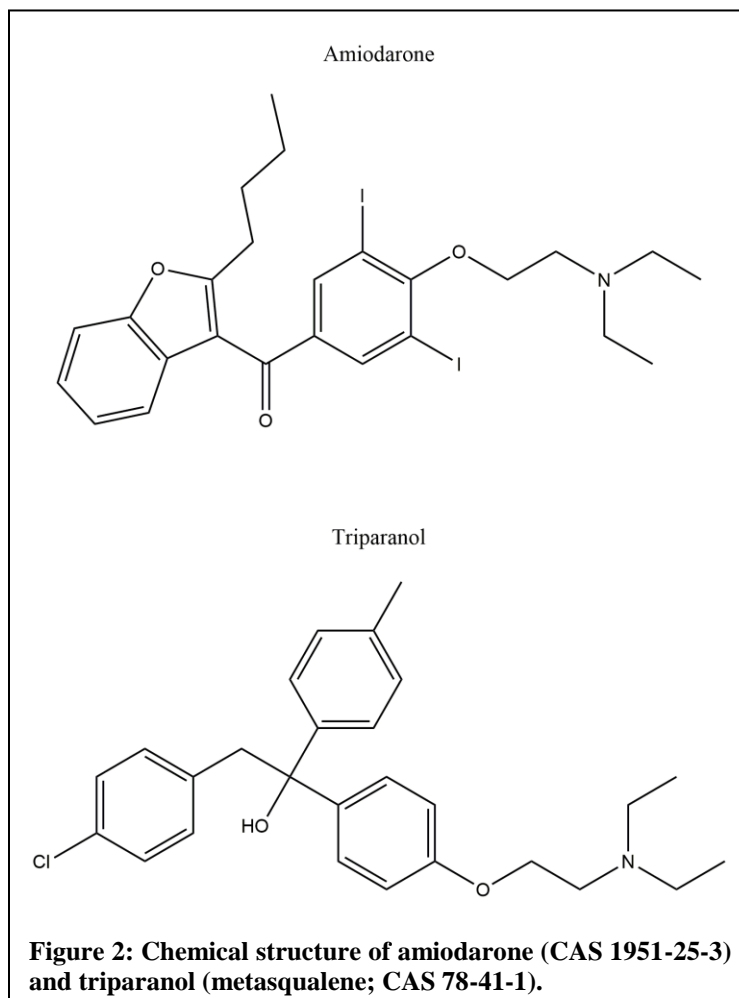
contraindicated for use during pregnancy but rather the American College of Obstetricians and Gynecologists recommends individualized therapy during pregnancy [71]. A review of literature on the use of pharmaceutical inhibitors showed that the inhibitors of Dhcr7 are teratogenic [43]. These examples illustrate the unintended consequences and side effects of various medications currently in use. While beneficial to patients with psychiatric disorders, a special caution should be taken when aripiprazole is prescribed to pregnant women.

In an effort to identify other pharmaceutical and experimental drugs that have off-target effects on cholesterol biosynthesis, our laboratory performed a series high-throughput screenings over the last several years. In total, we have profiled the effects of about 3,000 compounds on cholesterol biosynthesis in various cell culture models [66-68]. These studies concluded that 5 to 10% of all compounds interfere with one of the enzymatic steps in post-lanosterol biosynthesis pathway. Considering that there are eight known genetic diseases caused by the mutations in sterol enzymes [72], it is alarming evidence that the use of various medications not intended to affect cholesterol metabolism, may lead to potentially severe clinical consequences related to the inhibition of sterol biosynthetic enzymes.

Amiodarone is commonly used to treat a variety of cardiovascular conditions and it was recognized that it might affect total cholesterol levels [73, 74]. However, only very recently it was reported that the users of amiodarone have greatly elevated desmosterol levels in their serum [75]. Interestingly, amiodarone's structure is strikingly similar to that of triparanol, with both containing a triethylamine moiety with an ether linkage to the rest of the compound (**Figure 2**). Of potential concern is one clinical case report about a child with developmental disabilities. After thorough exclusion of genetic causes, the only plausible identified cause was the use of amiodarone by mother during the pregnancy [76]. Thus, we designed the experiments to test the effects of amiodarone on cholesterol biosynthesis in a neuronal cell line, Neuro2a and in primary cultures of mouse neurons and astrocytes.

Effects of amiodarone on cholesterol biosynthesis

Amiodarone is a commonly prescribed anti-arrhythmic drug predominantly used in the treatment of ventricular arrhythmias [77]. Additionally it is also used to treat other cardiovascular conditions including atrial fibrillation, atrial flutter, refractory atrioventricular nodal and atrioventricular re-entrant tachycardia. The primary action of amiodarone is blocking potassium rectifier currents in the heart [78]. Other actions of



amiodarone include effects on beta-adrenergic receptors, calcium and sodium channels. Amiodarone was the 198th most prescribed medication in the US in 2016 with 2.9 million prescriptions [79] and is on the World Health Organization list of essential medicines [80].

The starting dose for amiodarone is 800-1600 mg per day taken orally in a single dose for 1-3 weeks. The dosage is then decreased to 100-200 mg per day in a single dose for maintenance [81]. It is important to consider that the drug has a very long elimination half-life at 58 days on average [82], while its active metabolite mono-N-desethylamiodarone (MDEA) has a 36 day half-life, though it may not reach steady state levels for up to a year [83]. Both amiodarone and MDEA accumulate in adipose tissue as well as the liver and lungs. Due to the long half-life and this accumulation in multiple tissues, the adverse effects of amiodarone may take several months to

relent upon cessation of the drug. In fact, the major risk factor for clinically significant toxic side effects identified by a retrospective study of amiodarone users' medical records was duration of treatment, with 1.6-2.8% of users being affected [84].

The most commonly listed side effect of amiodarone use is corneal microdeposits which occur in most users, followed by cardiac, pulmonary and liver toxicity as well as hypo- and hyperthyroidism. Dermatologic effects such as blue skin discoloration and photosensitivity have also been reported [77]. Neurologic toxicity symptoms range from cognitive impairment to peripheral neuropathy, ataxia and in rare cases, quadriplegia. We were interested to determine if the neurological toxicity might be related to the ability of amiodarone to alter cholesterol synthesis.

Recent studies showed that the most affected pathway in rats treated with amiodarone was cholesterol biosynthesis [73, 74, 85]. This is an interesting observation considering the importance of cholesterol for maintaining membrane fluidity and composition. Both of these aspects may then affect the functioning of potassium channels and other membrane proteins [86]. Amiodarone is capable of crossing the blood brain barrier and due to the brain's reliance on *de novo* cholesterol biosynthesis, perturbation of this process by prescription drugs is necessary to consider when attempting to understand the etiology of off-target effects. Since the mechanism by which amiodarone alters cholesterol biosynthesis is unknown, further analysis of amiodarone's effects on cholesterol synthesis may help to elucidate this mechanism. Here we show the effects of amiodarone on neuronal and glial sterol synthesis and examine the sterol composition in serum of amiodarone users.

CHAPTER 2: METHODS

Mouse studies

Adult mice, B6.129S5-*Dhcr24*^{tm1lex/Sbpaj}, stock no: 012564 and B6.129P2(Cg)-*Dhcr7*^{tm1GstJ}, stock no: 007453 were purchased from the Jackson Laboratory. The mice were housed under a 12-hr light-dark cycle at constant temperature (25 °C) and humidity with *ad libitum* access to food and water in Comparative Medicine at UNMC, Omaha, NE. Embryonic and newborn mice from Het (*Dhcr24*^{+/-}) x Het (*Dhcr24*^{+/-}) and Het (*Dhcr7*^{+/-}) x Het (*Dhcr7*^{+/-}) matings were used for the study. The whole brain was dissected then bisected along the longitudinal fissure prior to freezing in 2-methyl butane pre-chilled on dry ice and stored at -80°C. Tail clips were collected for genotype confirmation. Half of the brain was used for sterol analysis and the other half was used for either total RNA extraction and qPCR or protein extraction and western blotting. All procedures were performed in accordance with the Guide for the Humane Use and Care of Laboratory Animals. The use of mice in this study was approved by the Institutional Animal Care and Use Committee of UNMC.

Study population

Serum samples were obtained from the Nebraska Biobank, a repository comprised of residual samples from patients who consent to donate any blood, serum or plasma left-over after laboratory testing. The Nebraska Biobank serves UNMC faculty as part of the Center for Clinical and Translational Research. The Biobank contains de-identified serum, plasma, and genomic DNA from consented patients' residual clinical laboratory samples. De-identified data is available for all samples and includes demographics, encounters, diagnoses, problem list, medications, procedures (including labs), and OB/GYN data. The Nebraska Biobank functions as a fee for service core facility at UNMC and is available to all NU System faculty at a subsidized rate. Electronic Health Record personnel identified a group of samples from users of amiodarone and an age and sex matched control group. The use of Biobank de-identified samples is not subject to regulations and as such does not require review and approval by the IRB.

Primary neuronal cultures

Primary cortical neuronal cultures were prepared from WT E15 mice. Pregnant females were anesthetized by isoflurane and sacrificed by decapitation. Embryos were dissected out and sacrificed by decapitation immediately after removal from the uterus. The brain was placed in pre-chilled HBSS solution (w/o Ca^{2+} , w/o Mg^{2+}) and cerebral cortices were dissected, meninges removed and cut into small chunks of similar sizes and transferred to Trypsin/EDTA (0.5%) (VWR International) for 25 min at 37°C . Following the incubation, trypsin solution was replaced with trypsin inhibitor (Sigma) solution and the tissue was centrifuged for 5 minutes. Tissue pieces were resuspended in Neurobasal medium with B-27 (Thermo Fisher Scientific) supplement and triturated with a fire-polished Pasteur pipette. The cells were pelleted by centrifugation for 5 min at 80 X g. The cell pellet was resuspended in Neurobasal medium with B-27 supplement and the cells were counted. The cells were plated on a poly-D-lysine coated 96-well plate at density 50,000 cells/well. The growth medium was Neurobasal medium plus B-27 supplement plus Glutamax (Thermo Fisher Scientific) plus $3\ \mu\text{M}$ cytosine arabinoside. Incubation was in the cell culture incubator (37°C , 5% CO_2) for 3 – 6 days. At the end of incubation, the cultures were processed for immunocytochemistry.

Primary astrocytic cultures

After plating the required number of cells for neuronal cultures, left-over cells were plated in 100 mm dishes at density of 10×10^6 per tissue culture plate in DMEM with 10% FBS. Under these conditions, astrocytes adhere and divide and completely populate the plate within 10-14 days. Once the plates were full, they were rinsed using the cold jet method [87], briefly 4°C media was pipetted over the cells to detach non-astrocytic cells, leaving only adherent astrocytes. The astrocytes were trypsinized and plated in 96-well plates in DMEM plus 10% FBS at 30,000 cells/well. The following day the medium was completely changed and astrocytes were grown in Neurobasal medium with B-27 supplement in the absence of cholesterol (same medium as neuronal

cells without cytosine arabinoside). Cells were incubated at 37°C, 5% CO₂ for 6 days. At the endpoint of incubation, cells were counted as described in a later section.

Control Neuro2a and *Ebp*-deficient Neuro2a cultures

The neuroblastoma cell line, Neuro2a, was purchased from ATCC (Rockville, MD). *EPB*-deficient Neuro2a cells were generated by *Ebp* shRNA (Open Biosystems) transfection. A stable cell line expressing *Ebp* shRNA was established using puromycin selection. The controls for *Ebp*-deficient Neuro2a cells were Neuro2a cells transfected with *non-silencing* shRNA and Neuro2a transfected with an empty plasmid. The cell lines were maintained in EMEM supplemented with L-glutamine, 10% FBS, and penicillin/streptomycin at 37°C and 5% CO₂ (plus puromycin for *Ebp*-deficient Neuro2a cells, *non-silencing* Neuro2a and empty plasmid Neuro2a). Cells were subcultured once a week and the culture medium changed every 2 days. For experimental purposes, the cells were plated in either 100 mm plates (protein extraction and RNA isolation), or 96-well plates (for sterol analysis and immunocytochemistry). To assess the endogenous sterol synthesis, these cultures were grown in defined medium without cholesterol and without lipids by using EMEM with N2 supplement, L-glutamine, and penicillin/streptomycin (plus/minus puromycin). At specific times, the cells were harvested from 100mm plates by removing medium, washing once with 5 mL 1X PBS, and then scraping cells with a spatula in 5mL 1X PBS. Cells were centrifuged for 8 min at 700 rpm at 4°C and PBS was removed before RNA isolation or protein extraction.

Immunocytochemistry and imaging

Neurite outgrowth of E15 neuronal cultures was evaluated on an ImageXpress Pico Automated Cell Imaging System using a 20X Fluotar objective in the Cy3 channel. Images were acquired and analyzed with CellReporterXpress software (Molecular Devices). For each well 49 individual fields were captured and stitched together. The neurite growth was analyzed by the neurite tracing algorithm in CellReporterXpress.

RNA isolation and clean-up

Brains were dissected from P0 pups and homogenized in 1 mL of ice cold TRIzol Reagent (Thermo Fisher Scientific). RNA was isolated following the protocol included with the TRIzol Reagent. RNA pellets were redissolved in nuclease-free water. RNA concentration and quality were measured using a NanoDrop 2000 Spectrophotometer (Thermo Fisher Scientific). 100 µg of isolated RNA was then cleaned using Qiagen's RNeasy Mini Kit following the manufacturer's protocol, including the on-column DNase digestion. RNA quality and quantity were measured again following the cleanup protocol.

Complementary DNA synthesis and RT² Profiler PCR Mouse Arrays

500 ng of total RNA was reverse transcribed using the First Strand cDNA Synthesis Kit (Qiagen) following the manufacturer's protocol. PCR data were collected by the StepOne Software v2.3 (Thermo Fisher Scientific) and analyzed by Qiagen's PCR Array Data Analysis Web Portal. Several methods to normalize gene expression changes were used, including the best fit from the panel of housekeeping genes and geometric mean from the full plate. Only gene expression changes that were statistically significant with all normalization protocols are presented in the Chapter 3.

Western blotting

Whole brain samples of *Dhcr24*^{+/+}, *Dhcr24*^{-/-} and *Dhcr24*^{+/-} newborn mice were homogenized by sonication in ice-cold RIPA lysis buffer (VWR International) plus phosphatase inhibitors (Sigma-Aldrich) and protease inhibitors (Thermo Fisher Scientific) and incubated on ice for 30 min. To clear the lysates, the samples were spun at 14,000 X g at 4°C for 5 min to pellet the debris. The protein concentration of the supernatant was quantified by PierceTM BCA Assay (Thermo Fisher Scientific). Equal amounts of protein from each sample were mixed with reducing reagent and loading buffer and heated to 70°C for 10 min. Proteins were separated on NuPAGETM 4-12% Bis-Tris Protein Gels (Thermo Fisher Scientific). Pre-stained protein was used to evaluate the molecular weight. The Bio-Rad Mini Trans-Blot Electrophoretic Transfer Cell was used for the electrophoretic transfer using polyvinylidene difluoride membranes (Immobilon-P PVDF

Membrane, Sigma-Aldrich) and transfer buffer (25 mM Tris, 192 mM glycine and 20% (v/v) methanol (pH 8.3)). Following transfer, PVDF membranes were blocked in 5% milk in TBS (50 mM Tris-Cl, 150 mM NaCl, pH 7.5) with 0.05% Igepal (Spectrum Chemical) and incubated in primary antibody overnight at +4°C and secondary antibodies at room temperature for 1 hour. Membranes were probed with the following primary antibodies: anti-DHCR24 (Cell Signaling), anti-beta-actin (Cell Signaling), anti-GAPDH (Cell Signaling) and anti-MAP2 (Cell Signaling). Western blots were developed using Azure's Radiance Substrate, imaged on an Azure C300 with the cSeries Capture Software and saved as TIFF images (Azure Biosystems). The TIFF images were analyzed with AzureSpot and data graphed in GraphPad Prism 8 (GraphPad Software).

Cell counting

Cells were counted on an ImageXpress Pico Automated Cell Imaging System at 4X Fluotar objective in the DAPI channel. To stain the nucleus, 100 µL of a 1:2000 dilution of Hoechst dye (Thermo Fisher Scientific) in PBS was added to each well and incubated for 5 minutes before data acquisition. Cells were counted using the cell counting algorithm in CellReporterXpress.

Sterol extraction for HPLC-MS/MS analysis

Tissue

Brains were homogenized in ice-cold 1X PBS using a Q55 sonicator (Qsonica). To a 5 µL aliquot of homogenate, Folch's solution (600 µL; 2/1 chloroform/methanol), aqueous NaCl solution (0.9%, 300 µL) and 10 µL of an internal standard mix (30 µM D₇-cholesterol, D₇-7-DHC, D₇-8-DHC, ¹³C₃-desmosterol and ¹³C₃-lanosterol) were added. The samples were then vortexed for 1 min and centrifuged at 10,000 RCF for 10 min. The bottom organic phase was collected and dried in a Savant Integrated SpeedVac® System (Thermo Fisher Scientific) and then redissolved in 100 µL of MeOH and transferred to a mass spec compatible plate pre-deposited with 200 µg 4-Phenyl-1,2,4-triazoline-3,5-dione (PTAD) per well and sealed with Easy Pierce Heat Sealing Foil (Thermo Fisher Scientific). Values were normalized to total protein as quantified by Pierce™ BCA assay

(Thermo Fisher Scientific) reading absorbance at 562 nm using a Spectromax Plus 384 (Molecular Devices) and reported as nmol/mg protein.

Serum

To a 10 μ L aliquot of human serum, Folch's solution (600 μ L; 2/1 chloroform/methanol), aqueous NaCl solution (0.9%, 300 μ L) and 10 μ L of an internal standard mix (30 μ M D₇-cholesterol, D₇-7-DHC, D₇-8-DHC, ¹³C₃-desmosterol and ¹³C₃-lanosterol) were added. The samples were then processed as the tissue samples described above. Values were normalized to volume and reported as ng/ μ L serum.

Cell cultures

Sterol levels were analyzed in individual wells and, for most experiments, cellular levels correspond to 8-12 technical replicates. After removing the medium, 200 μ L of MeOH containing internal standard (30 μ M D₇-cholesterol, D₇-7-DHC, D₇-8-DHC, ¹³C₃-desmosterol and ¹³C₃-lanosterol) were added. The 96-well plates were placed on an orbital shaker for 30 min at room temperature. An aliquot (100 μ L) of the supernatant was transferred to a PTAD-predeposited plate, sealed with Easy Pierce Heat Sealing Foil followed by 30 min agitation at room temperature and analyzed by LC-MS/MS. Values were normalized by cell count per well and reported as nmol/million cells.

HPLC-MS/MS (SRM) analyses of sterols

The samples were placed on an Acquity UPLC system coupled to a Thermo Scientific TSQ Quantis mass spectrometer equipped with an APCI source. Then 5 μ L was injected onto the column (Acquity BEH C18 1.7 μ m, 2.1 mm \times 50 mm) with 100% MeOH (0.1% v/v acetic acid) mobile phase for 1.0 min runtime at a flow rate of 500 μ L/min. Natural sterols were analyzed by selective reaction monitoring (SRM) using the following *m/z* transitions: cholesterol 369 \rightarrow 369, 7-DHC 560 \rightarrow 365, 8-DHC 558 \rightarrow 363, desmosterol 592 \rightarrow 560, lanosterol 634 \rightarrow 602, with retention times of 0.7, 0.4, 0.4, 0.3 and 0.3 min, respectively. SRMs for the internal standards were set to: d₇-Chol

376 → 376, d₇-7-DHC 567 → 372, d₇-8-DHC 565 → 370, ¹³C-desmosterol 595 → 563, ¹³C-lanosterol 637 → 605.

Sterol extraction for GC-MS analysis of sterols

Serum

To a 10 μL aliquot of human serum, Folch's solution (600 μL; 2/1 chloroform/methanol), aqueous NaCl solution (0.9%, 300 μL) and 10 μL of an internal standard mix (30 μM D₇-cholesterol, D₇-7-DHC, D₇-8-DHC) were added. The samples were then vortexed for 1 min and centrifuged at 10,000 RCF for 10 min. The bottom organic phase was collected in a glass autosampler vial and dried in a Savant Integrated SpeedVac® System (Thermo Fisher Scientific). Dried lipid samples were derivatized with 35 μL N,O-bis(trimethylsilyl)trifluoroacetamide (BSTFA) and transferred to a glass autosampler vial insert for analysis. Values were normalized by volume of serum and reported as ng/μL of serum.

Cell cultures

Single wells were extracted with 200 μL of MeOH containing an internal standard cocktail (30 μM D₇-cholesterol, D₇-7-DHC, D₇-8-DHC). An aliquot (190 μL) of the supernatant was transferred to glass autosampler vial. Three adjacent wells were combined in each vial before drying. Samples were dried in a SpeedVac concentrator. Dried lipid samples were derivatized with BSTFA and transferred to a glass autosampler vial insert for analysis. Values were normalized by average cell count and reported as fold change over control (DMSO for amiodarone, *non-silencing* shRNA for *Ebp*-deficient Neuro2a).

GC-MS analysis of sterols

5 μL of BSTFA-derivatized lipid sample was injected onto the column (SPB-5, 0.25 μm, 0.32 mm × 30 m) with the following temperature program: 180°C was held for 1 min; then increased to 250 °C at 20°C/min; then raised to 300°C at 4°C/min and kept for 7 min. Selected sterol intermediates were analyzed by extracted ion chromatogram (EIC) using the following

values: cholesterol (m/z 458, retention time 16.9 min), zymostenol (m/z 458, retention time 17.1 min), zymosterol (m/z 456, retention time 17.4 min) and D₇-Chol (m/z 465, retention time 16.9 min). Final sterol numbers were calculated using D₇-Chol as the internal standard. Response factors were calculated for each sterol and used to calculate the total amount.

Serum drug extraction

To 75 μ L of human serum were added 188 μ L H₂O, 10 μ L internal standard (d₈-aripiprazole) and 75 μ L of 4.5 M ammonium hydroxide. The samples were then vortexed vigorously for 1 minute. Following vortexing, 950 μ L of methyl *tert*-butyl ether (MTBE) was added to each sample followed by another minute of vortexing. Samples were then centrifuged at 10,000 RCF for 10 minutes. The top organic layer was collected to a glass autosampler vial and dried in a SpeedVac. After samples were dried 150 μ L of MeOH/NH₃•H₂O (95:5, v/v) was added to each vial, briefly vortexed and then transferred to a chromatography vial insert for LC-MS/MS analysis.

Serum drug measurements

Amiodarone and MDEA levels were acquired on an Acquity UPLC system coupled to a Thermo Scientific TSQ Quantis mass spectrometer using an ESI source in the positive ion mode. 5 μ L of each sample was injected onto the column (Phenomenex Luna Omega C18, 1.6 μ m, 100 Å, 2.1 mm \times 50 mm) using water (0.1% v/v acetic acid) (solvent A) and acetonitrile (0.1% v/v acetic acid) (solvent B) as mobile phase. The gradient was: 10% to 40% B for 0.5 min; 40% to 95% B for 0.4 min; 95% B for 1.5 min; 95% to 10% B for 0.1 min; 10% B for 0.5 min. Amiodarone and MDEA levels were analyzed by selective reaction monitoring (SRM) using the following m/z transitions: amiodarone 646 \rightarrow 86, and MDEA 618 \rightarrow 72. The SRM for the internal standard (d₈-aripiprazole) was set to 456 \rightarrow 293 and response factors were determined to accurately determine the drug levels. Final drug levels are reported as ng/mL of serum.

Statistical analyses

Data are presented as the mean \pm standard error of the mean. Unpaired two-tailed t-tests were performed for individual comparisons between two groups, employing Welch's correction

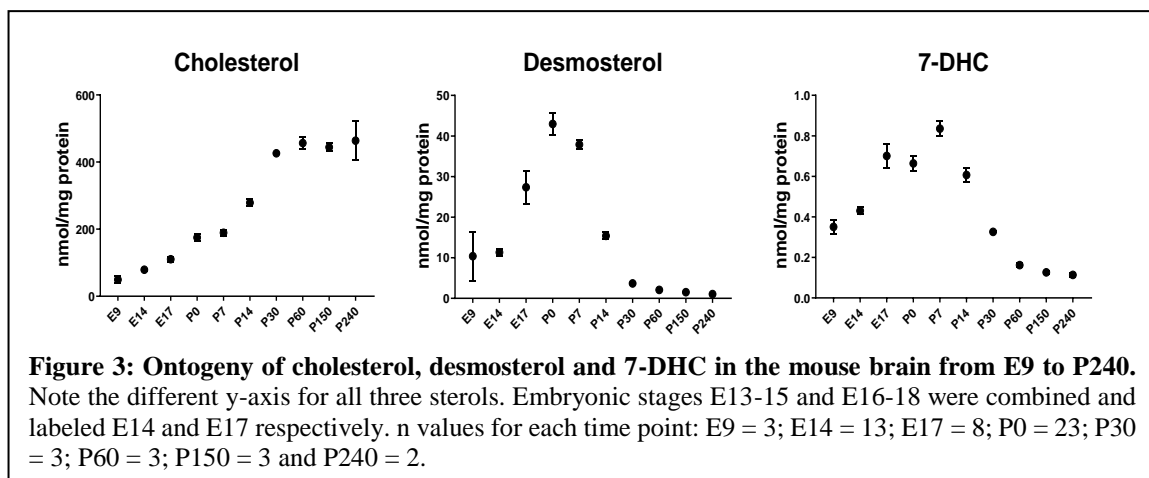
when the variances between the two groups were significantly different. A one-way ANOVA with multiple comparisons and Tukey corrections were performed for comparisons between three or more groups. The P values for statistically significant differences are highlighted in Figure Legends. Statistical analyses were performed using GraphPad Prism version 8 (GraphPad Software) for Windows and Microsoft Excel 2016.

CHAPTER 3: RESULTS

Cholesterol, desmosterol and 7-DHC levels show a developmental trajectory

Cholesterol is the major sterol in brain tissue and starts accumulating early in embryonic development. However, the temporal production of cholesterol and its two immediate precursors (desmosterol and 7-DHC) in the brain is not well understood to date. To gain insight into this process, we compared the levels of cholesterol and its immediate precursors starting from embryonic stages (E9) to adulthood (P240) in the brain (**Figure 3**).

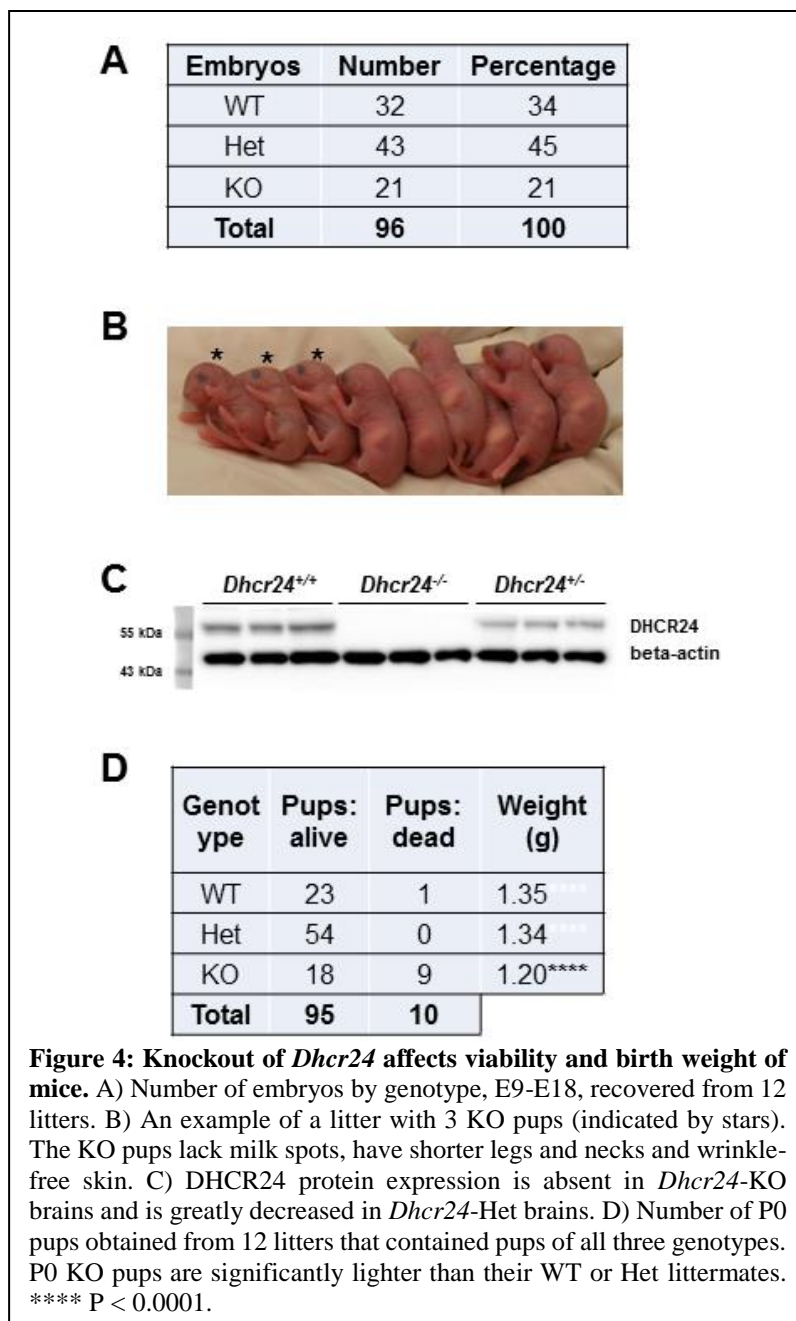
We found that compared to cholesterol, the absolute levels of its precursors were significantly lower at all stages of development: cholesterol was an order of magnitude more abundant than desmosterol, while desmosterol was an order of magnitude higher than 7-DHC. Cholesterol, desmosterol and 7-DHC each had a distinct developmental trajectory. The most significant increase in cholesterol levels was observed from E17 to P30, with levels plateauing thereafter. Desmosterol levels increased linearly from E9 through P0 and after P30 stayed at low levels. In contrast, 7-DHC was present at very low levels in the mouse brains, peaking at P7 and declining thereafter.



Cholesterol deficiency leads to early postnatal death

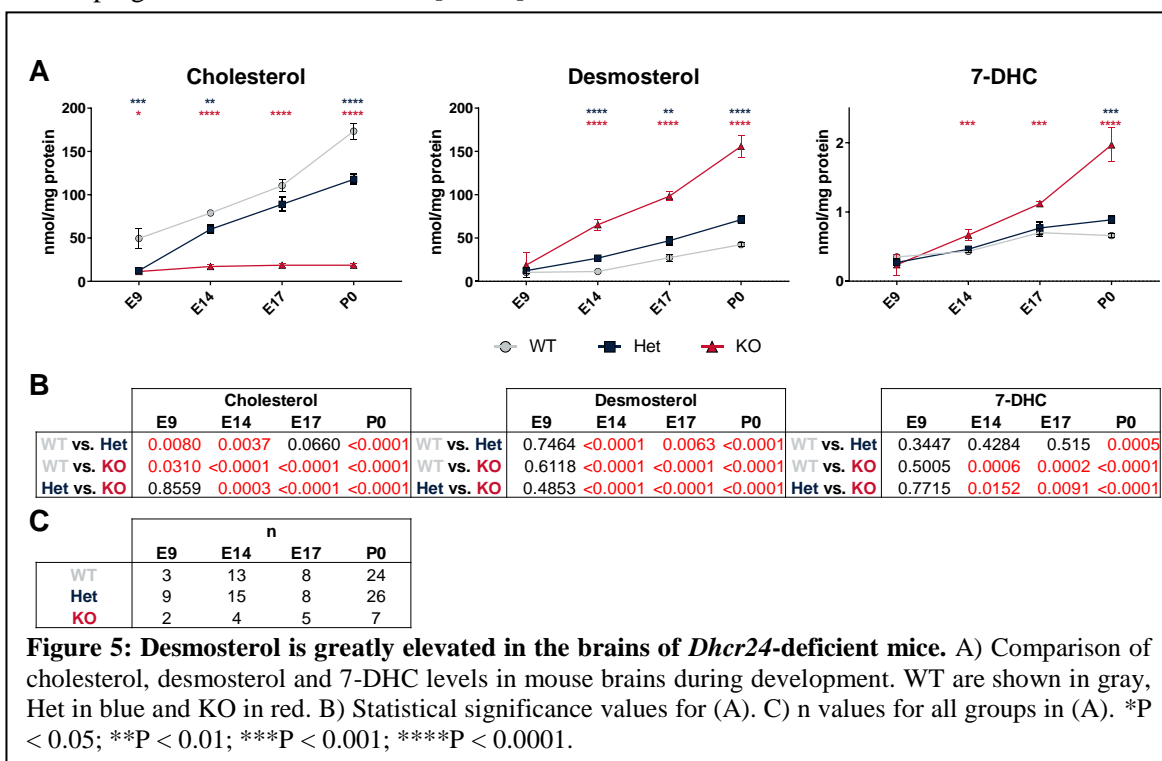
Desmosterolosis is an autosomal recessive disorder with Mendelian inheritance, thus the expected frequency of knockouts is approximately 25%. In our mouse colony we found a slightly lower than expected number of *Dhcr24*-KO mice (**Figure 4A**): in 12 litters with total 96 embryos (average number of embryos per litter = 8) we obtained 21% of KOs. At P0, *Dhcr24*-KO pups could be visually identified by lack of wrinkled skin, shorter limbs and a missing a milk spot

(**Figure 4B**). Western blot analyses of P0 brains revealed DHCR24 protein was completely absent in *Dhcr24*-KO pups, while *Dhcr24*-Het mice brains revealed a 50% reduction of DHCR24 when compared to WT littermates (**Figure 4C**). At P0, in addition to commonly observed KO stillborn pups (9 stillborn out of 27 born), all live-born KO pups died shortly after birth. Furthermore, KO pups weighed approximately 10% less than WT littermates ($P < 0.0001$), while WT and *Dhcr24*-Het P0 weights were comparable (**Figure 4D**).



Desmosterol is greatly elevated in the brains of *Dhcr24*-deficient mice

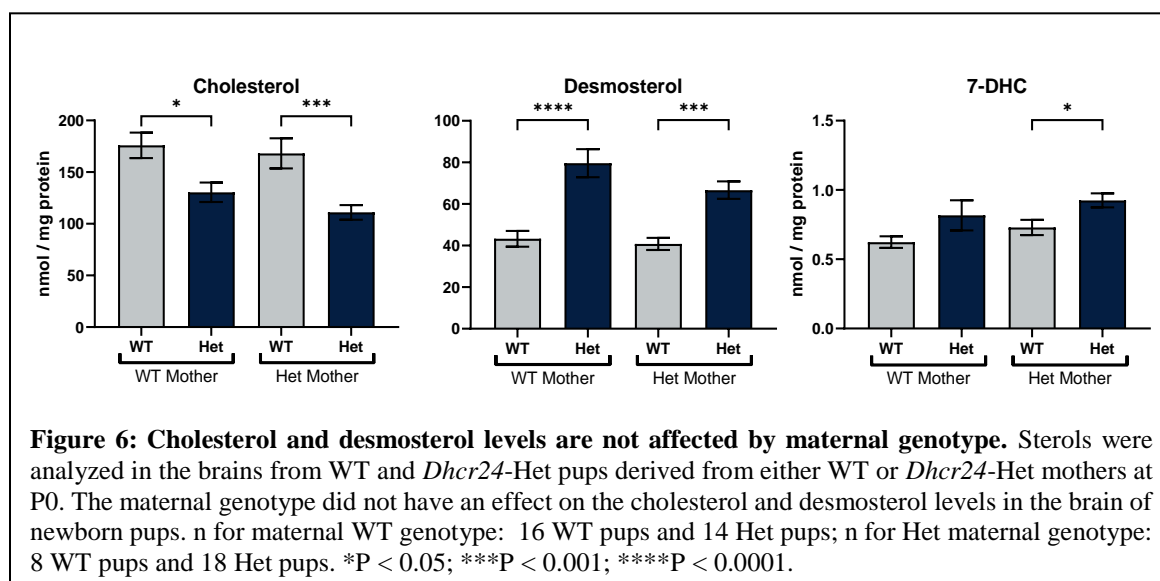
Next, we compared cholesterol, desmosterol and 7-DHC levels in brains of WT, Het and *Dhcr24*-KO littermates during embryonic development and shortly after birth (**Figure 5**). While there was a steady increase of cholesterol and desmosterol in the WT and Het brains during embryonic stages, no accumulation of cholesterol in *Dhcr24*-KOs could be observed. Instead, desmosterol steadily accumulated in embryonic KO brains, reaching comparable levels to that of cholesterol seen in the WT brains by P0. Interestingly, the difference among WT, Het and *Dhcr24*-KO sterol levels was already present at E14, with the most pronounced differences at P0. Our results also confirmed previously reported data that endogenous brain cholesterol synthesis in the developing brain starts around E12 [88, 89].



Desmosterol is elevated in *Dhcr24*-Het mice compared to WT littermates

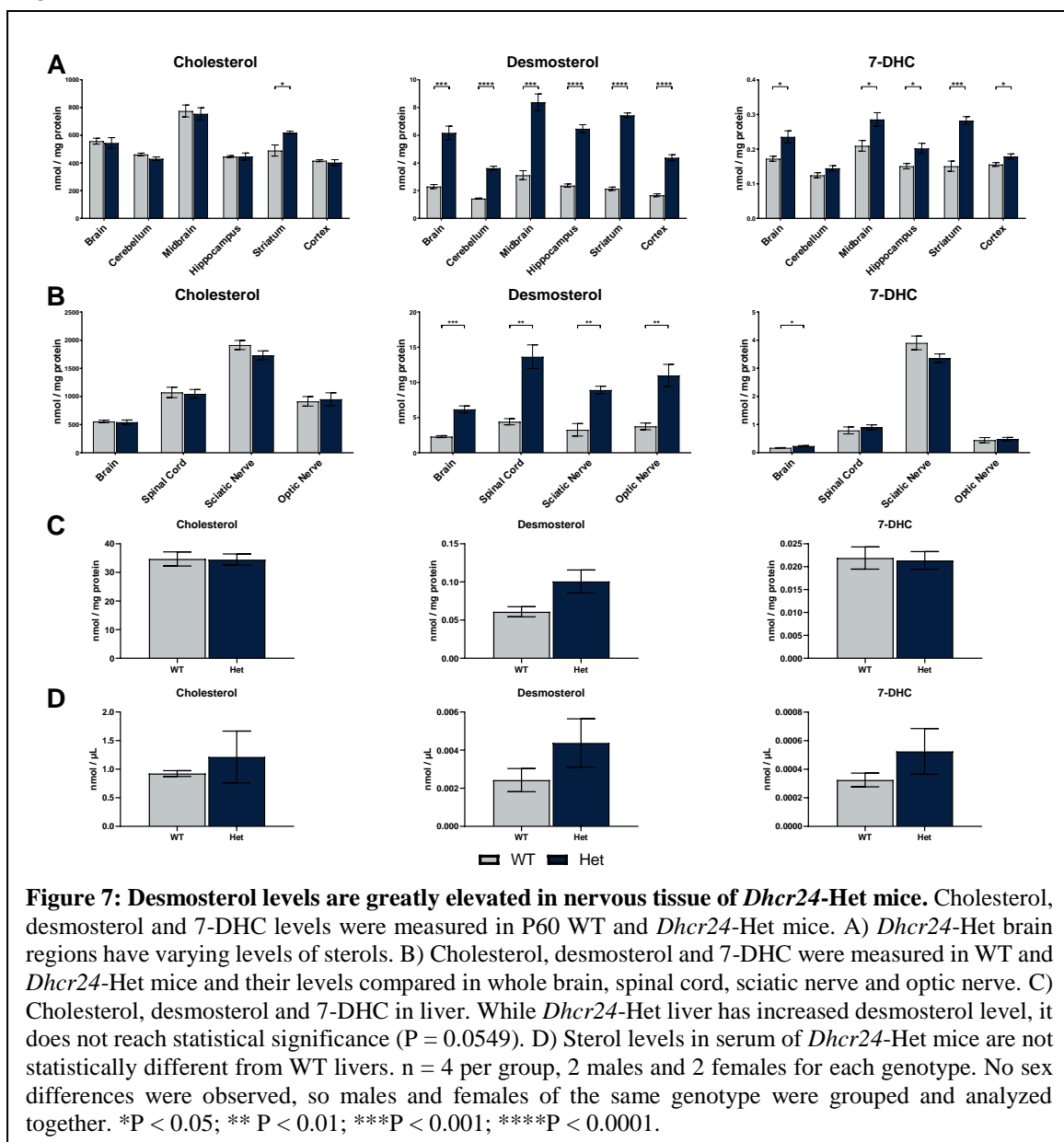
Since we found that desmosterol is significantly elevated in P0 brain of *Dhcr24*-Het mice, we hypothesized that in these mice *i*) elevated desmosterol levels will persist into adulthood, and *ii*) maternal Het genotype will by itself have an effect on the developing pups. The effect of the maternal genotype on the pup's brain sterol levels is shown in **Figure 6**. We found decreased

cholesterol ($P < 0.001$) and increased desmosterol ($P < 0.01$) levels in the brain tissue of *Dhcr24*-Het pups, which was independent of the maternal genotype (e.g. *Dhcr24*-Het pups originating from *Dhcr24*-Het vs WT mothers). In addition, we observed that 7-DHC levels were elevated in Het pups compared to their WT littermates in litters from Het mothers only ($P = 0.0280$). However, at present, the biological significance of such a small elevation in 7-DHC is unclear.



Next, desmosterol, 7-DHC and cholesterol levels were compared across different brain regions and the whole brain of two-month-old WT and *Dhcr24*-Het mice. While there was a significant difference in cholesterol levels between WT and Het brains at P0, no difference was detected at P60 across the analyzed brain regions, except in the striatum, which showed elevated cholesterol levels (**Figure 7A**). In contrast, desmosterol levels remained greatly elevated at P60 in all brain regions, with the most pronounced increase in the striatum (**Figure 7A**). Surprisingly, the largest difference in 7-DHC levels was observed at P60, with the most pronounced changes in the striatum. In addition to brain tissue, several other tissues were analyzed at P60. These include spinal cord, sciatic and optic nerve (**Figure 7B**) as well as liver (**Figure 7C**) and serum (**Figure 7D**). Compared to the brain, the serum had the lowest levels of sterols, while the spinal cord, sciatic and

optic nerves had a larger amount of sterols. It should be noted that all nervous tissue had much higher levels of the three sterols than the liver or serum in both WT and Het mice.



Elevated desmosterol levels result in complex transcriptional changes

Since sterols are potent regulators of gene expression [90, 91], we screened P0 brain tissue using specific PCR arrays (Qiagen) to determine if elevated desmosterol changes gene expression. The pathway-focused panels used in this study include lipoprotein signaling and cholesterol metabolism, nuclear receptors and coregulators and synaptic plasticity arrays. The screening of both *Dhcr24*-KO and *Dhcr7*-KO brain tissues was done to compare similarities and differences.

The full list of differentially regulated transcripts and their function is shown in **Table 1**. Six lipid transcripts were downregulated and four were upregulated in *Dhcr24*-KO brain. Among the lipid transcripts, *Dhcr24* was undetectable in *Dhcr24*-KO brains, and *Dhcr7* transcript was undetectable in *Dhcr7*-KO brains. Among lipid transcripts with altered expression in *Dhcr24*-KO brains, three were also changed in the brains of *Dhcr7*-KO mice, albeit in the opposing direction. These three included *Srebfl*, a transcription factor and two sterol transporters, *Abca1* and *Abcg1*. These findings are in agreement with elegant studies by Yang et al [92] showing that desmosterol regulates expression of *Abca1* through the activation of LXRs.

Among transcripts encoding nuclear receptors and co-regulators we identified eight transcripts with downregulated expression in *Dhcr24*-KO mice and two transcripts altered in *Dhcr7*-KO brains (one downregulated and one upregulated). Common between the two disorders was downregulation of *Nr2f2*, a transcription factor. While all nuclear receptors were downregulated in *Dhcr24*-KO brain, synaptic plasticity transcripts were all upregulated. Of these four upregulated genes for synaptic plasticity, one encodes a neural cell adhesion molecule, while the remaining three are transcription factors with expression patterns ranging from ubiquitous to highly region-specific expression in the brain. To determine if there is a common dysregulated pathway and visualize the interaction among various transcripts, all genes with altered expression were uploaded into the STRING database (<https://string-db.org/>). The visualization of interactions is shown in **Figure 8**. This expanded network analysis revealed that these genes had common interaction partners, suggesting that *Dhcr24*- and *Dhcr7*-deficiency might affect the same nuclear transcriptional network.

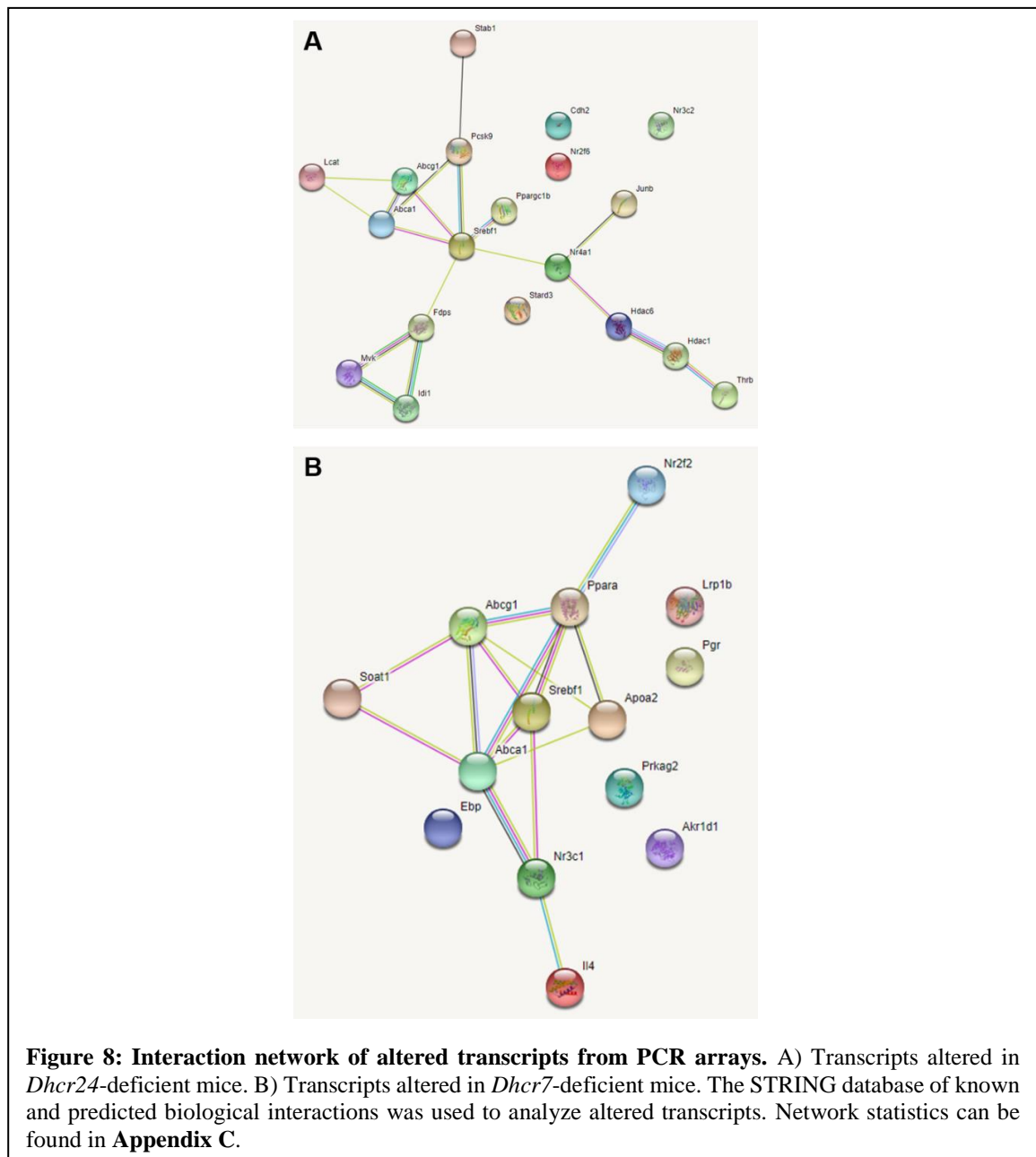
Table 1: Elevated desmosterol changes lipoprotein signaling, cholesterol biosynthesis transcripts, synaptic plasticity transcripts, nuclear receptors and coregulators. The table shows the gene symbol, gene name and biological function along with fold regulation and P values. The upregulated transcripts are shown in blue while downregulated transcripts are shown in red. All statistically significant changes are shown in red, $P < 0.05$.

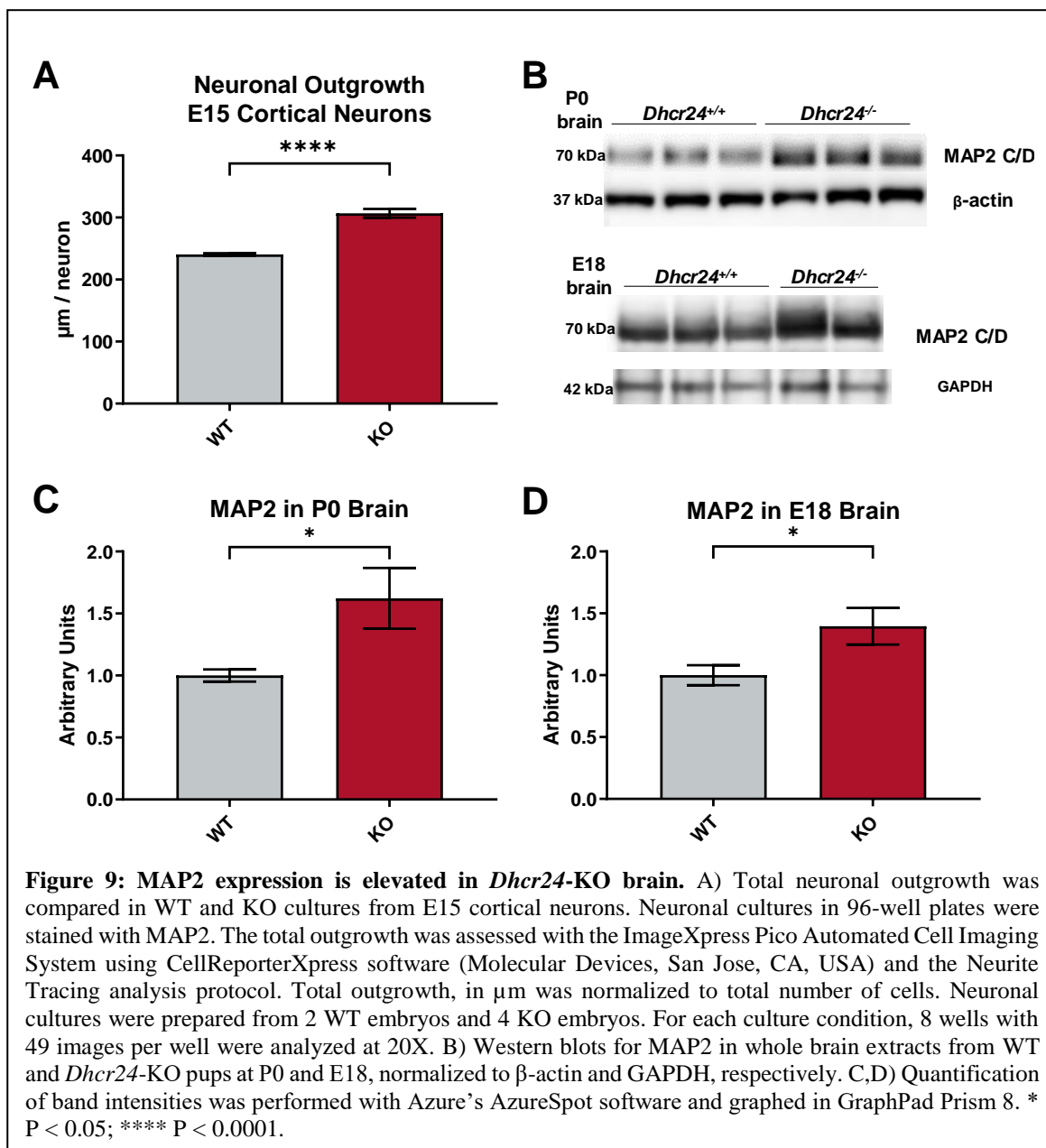
Gene and Function			DESMO		SLOS	
Gene Symbol	Gene Name	Function	Fold regulation	pValue	Fold regulation	pValue
Lipoproteins						
Abca1	ATP binding cassette subfamily A - 1	Lipid transport	1.44	0.017	-1.631	0.013
Abcg1	ATP binding cassette subfamily G - 1	Lipid transport	1.79	0.0003	-2.583	0.0003
Akr1d1	Aldo-keto reductase family 1 member D1	Bile acid synthesis	1.22	0.477	2.020	0.028
Apoa2	Apolipoprotein A2	Cholesterol homeostasis	-1.07	0.526	-1.375	0.001
Dhcr7	Dehydrocholesterol reductase 7	Cholesterol biosynthesis	-1.117	0.349	-1295.5	0.0005
Dhcr24	Dehydrocholesterol reductase 24	Cholesterol biosynthesis	-113.452	0.00006	-1.061	0.432
Fdps	Farnesyl diphosphate synthase	Isoprenoid biosynthesis	-1.371	0.002	-1.03	0.779
Il4	Interleukin 4	Immune response	1.024	0.875	1.978	0.049
Lcat	Lecithin-cholesterol acyltransferase	Lipoprotein metabolism	-1.174	0.021	-1.064	0.659
Mvk	Mevalonate kinase	Isoprenoid biosynthesis	-1.253	0.037	-1.219	0.105
Pesk9	Proprotein convertase subtilisin/kexin type 9	Cholesterol homeostasis	1.29	0.028	-1.197	0.098
Prkag2	Protein kinase AMP-activated non-catalytic subunit gamma 2	Cholesterol biosynthesis	-1.225	0.051	-1.262	0.023
Soat1	Sterol O-acyltransferase 2	Cholesterol homeostasis	-1.039	0.525	1.179	0.035
Srebf1	Sterol regulatory element binding transcription factor 1	Transcription factor	1.492	0.003	-1.814	0.007
Stab1	Stabilin 1	Lipoprotein metabolism	-1.321	0.028	1.105	0.39
Stard3	StAR related lipid transfer domain containing 3	Cholesterol metabolism	-1.216	0.002	-1.03	0.773
Nuclear Receptors and Coregulators						
Hdac1	Histone deacetylase 1	Transcriptional regulation	-1.350	0.034	-1.098	0.441
Hdac6	Histone deacetylase 6	Transcriptional regulation	-1.178	0.015	-1.127	0.120
Ncoa1	Nuclear receptor coactivator 1	Transcriptional regulation	-1.159	0.023	-1.104	0.241
Nr2f2	Nuclear receptor subfamily 2 group F member 2	Transcriptional regulation	-1.344	0.0178	-1.156	0.118
Nr2f6	Nuclear receptor subfamily 2 group F member 6	Transcriptional regulation	-1.208	0.006	-1.271	0.000568
Nr3c1	Nuclear receptor subfamily 3 group C member 1	Transcriptional regulation	-1.222	0.0153	-1.153	0.129
Ppara	Peroxisome proliferator activated receptor alpha	Transcriptional regulation	-1.186	0.382	1.264	0.033
Ppargclb	PPARG coactivator 1 beta	Transcriptional regulation	-1.271	0.024	-1.294	0.096
Thrb	Thyroid hormone receptor beta	Transcriptional regulation	-1.378	0.018	-1.169	0.133
Synaptic Plasticity						
Cdh2	Cadherin 2	Extracellular matrix	1.426	0.025	n.d.	
Cebpd	CCAAT/Enhancer binding protein delta	Transcription factor	3.268	0.004	n.d.	
Junb	Jun proto-oncogene	Transcription factor	1.929	0.043	n.d.	
Nr4a1	Nuclear receptor subfamily 4 group A member 1	Orphan nuclear receptor	2.025	0.039	1.6635	0.198

High desmosterol levels alter neuronal outgrowth

Synaptic development is a cholesterol-dependent process and altered sterol composition of neuronal membranes affects neuronal arborization. For example, in a SLOS mouse model, elevated 7-DHC increases dendritic and axonal length of hippocampal neurons [93] and 7-DHC derived oxysterols greatly increase neuronal arborization [94]. To test if elevated desmosterol has an effect on neuronal morphology, we prepared cortical neuronal cultures from embryonic day 15 (E15) *Dhcr24*-KO and WT brains. Neurons were cultured for up to six days and their morphology was

analyzed using the neuron-specific marker microtubule associated protein 2 (MAP2). Imaging and quantification of total neuronal outgrowth revealed that arborization of *Dhcr24*-KO neurons was significantly increased compared to the neuronal outgrowth seen in samples originating from WT brains ($P < 0.0001$) (**Figure 9A**). To corroborate these results, protein was extracted from E18 and P0 brains, followed by western blotting for MAP2 (**Figure 9B-D**). This experiment revealed that MAP2 was also greatly elevated in *Dhcr24*-KO brains at both E18 and P0, confirming the initially observed *in vitro* data.





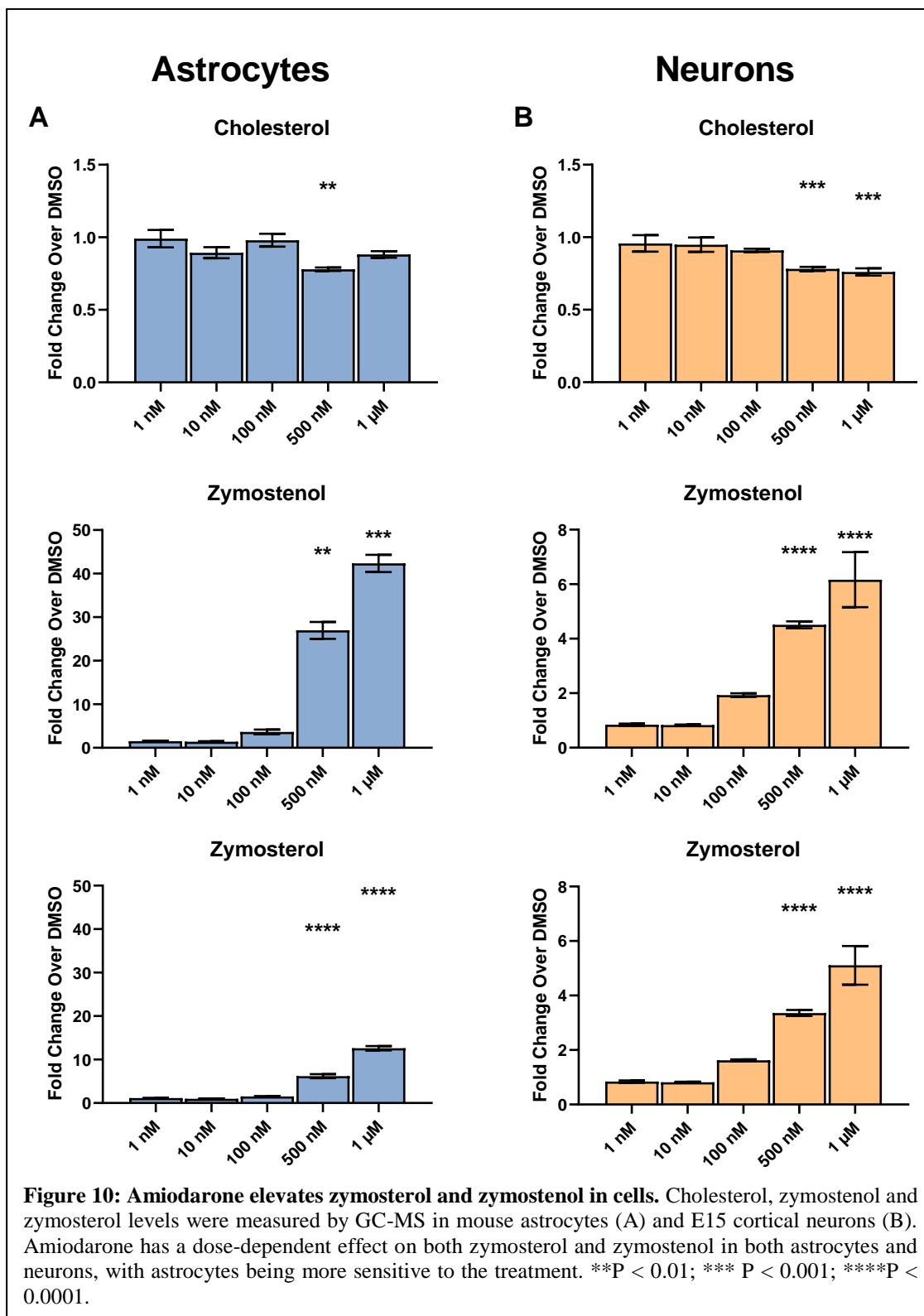
Amiodarone affects post-lanosterol cholesterol biosynthesis in neuronal and glial cells

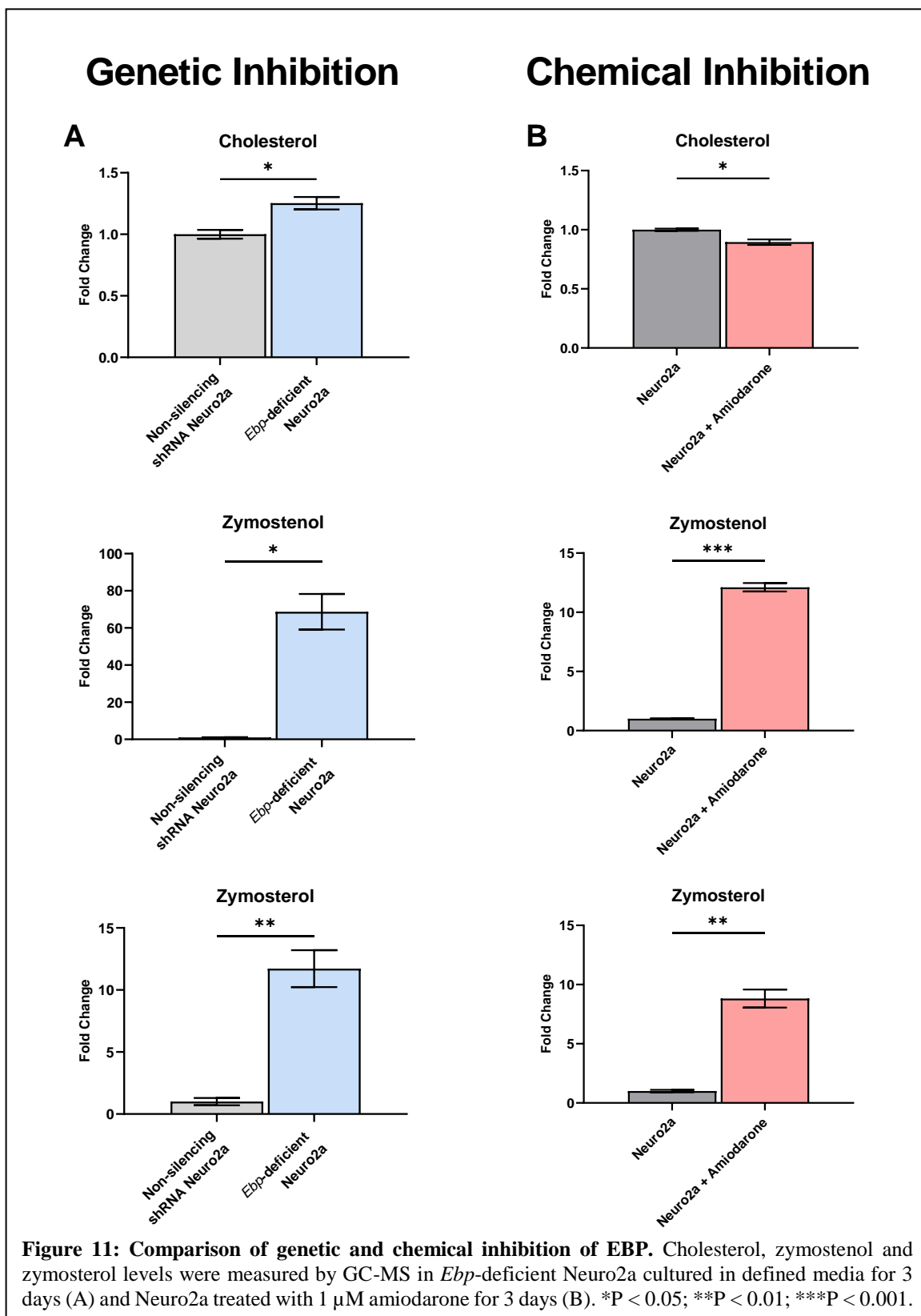
Amiodarone crosses the blood brain barrier and long-term use leads to an increased incidence in neurological symptoms including tremors, gait ataxia, peripheral neuropathy and cognitive impairment. Although the mechanism of action in the nervous system is currently unknown, several reports implicate altered cholesterol biosynthesis [73, 74, 85]. **Figure 1B** shows a schematic of post-lanosterol cholesterol biosynthesis including intermediates that were measured

in the present study. To assess the effects of amiodarone on post-lanosterol synthesis we treated primary cortical neurons and astrocytes with increasing concentrations of amiodarone and analyzed levels of sterol intermediates by LC-MS/MS and GC-MS. While cell viability was not affected over the range of concentrations used, several sterol intermediates were affected by the treatment. Notably cholesterol content was slightly decreased, with a more pronounced effect in neurons (**Figure 10B**) while zymostenol and zymosterol levels are drastically increased compared to DMSO treatment with the magnitude of increase being much larger in astrocytes (**Figure 10A**). The increase in zymostenol and zymosterol suggests that amiodarone inhibits Ebp, the enzyme responsible for the conversion of zymosterol to 24-dehydrodihydrocholesterol or zymostenol to dihydrocholesterol (**Figure 1**).

Amiodarone inhibits the sterol biosynthetic enzyme EBP

To confirm that amiodarone treatment produces a similar sterol profile when compared to EBP inhibition we generated an *Ebp*-knockdown Neuro2a cell line utilizing shRNA specific to EBP. These mouse neuroblastoma cells have been used extensively in cholesterol biosynthesis studies [66-68, 90, 95]. In fact, *Dhcr7*-deficient Neuro2a cells were key in elucidating the molecular defects associated with faulty cholesterol synthesis [90, 96]. Using the same methods as previously mentioned to measure sterol intermediate levels, we compared *Ebp*-deficient Neuro2a cells with amiodarone treated Neuro2a cells (**Figure 11**). While cholesterol levels are modulated in opposite directions with the two conditions, zymosterol and zymostenol show the same alteration. Note that while the magnitude of increase in zymosterol for both genetic and chemical inhibition are similar, the magnitude of change for zymostenol is much greater.





Amiodarone users have elevated serum levels of desmosterol, 8-DHC, zymosterol and zymostenol

Based on the findings from our cell culture experiments we wanted to determine if the changes in cholesterol biosynthesis were reflected in the serum of human patients taking the medication. Through the Nebraska Biobank we obtained de-identified serum samples from patients with amiodarone in their medical records as well as age- and sex-matched samples from control individuals. Of the 60 samples with amiodarone listed in the medical records we identified 14 samples that contained amiodarone and MDEA in measurable quantities via LC-MS/MS (**Figure 12A-C**). Of these 14 samples, 9 were given amiodarone orally (**Figure 12D, E**, gray boxes) while the remaining 5 received intravenous amiodarone (**Figure 12D, E**, red boxes). The samples that came from patients receiving amiodarone orally had higher levels of amiodarone and MDEA in their plasma on average.

We then analyzed cholesterol, desmosterol and 8-DHC content of the serum by LC-MS/MS and zymosterol and zymostenol content of the serum by GC-MS of the 14 amiodarone samples along with the matched controls (**Figure 13**). As previously reported, desmosterol was significantly increased in the amiodarone samples. Zymostenol showed a trend towards elevation in response to treatment. Zymosterol was also increased in the treated samples, although it was only detectable in 6 of 9 oral amiodarone samples and 1 out of 5 intravenous amiodarone samples. Interestingly, 8-DHC levels were also increased with amiodarone use, a finding that is consistent with the inhibition of EBP.

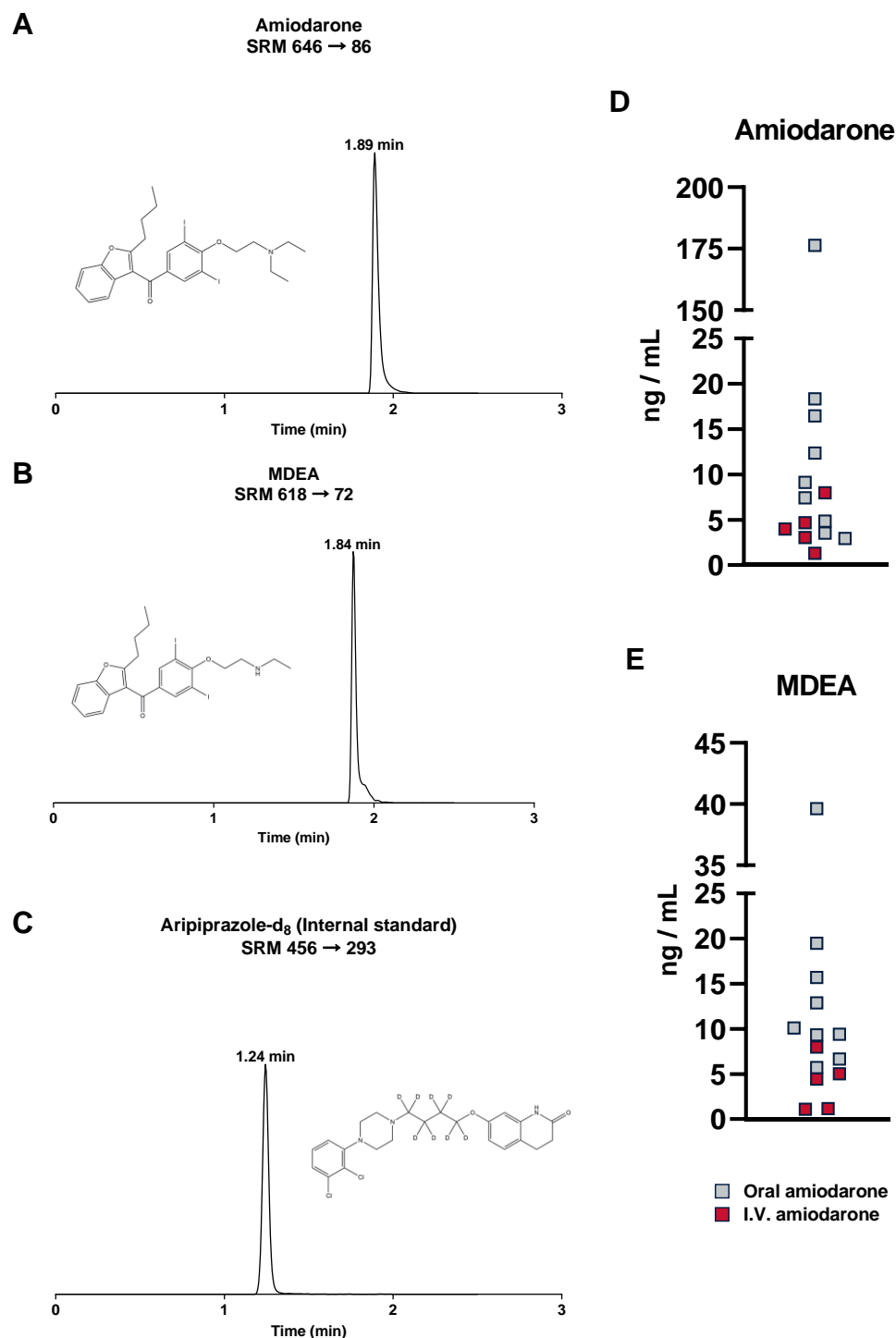
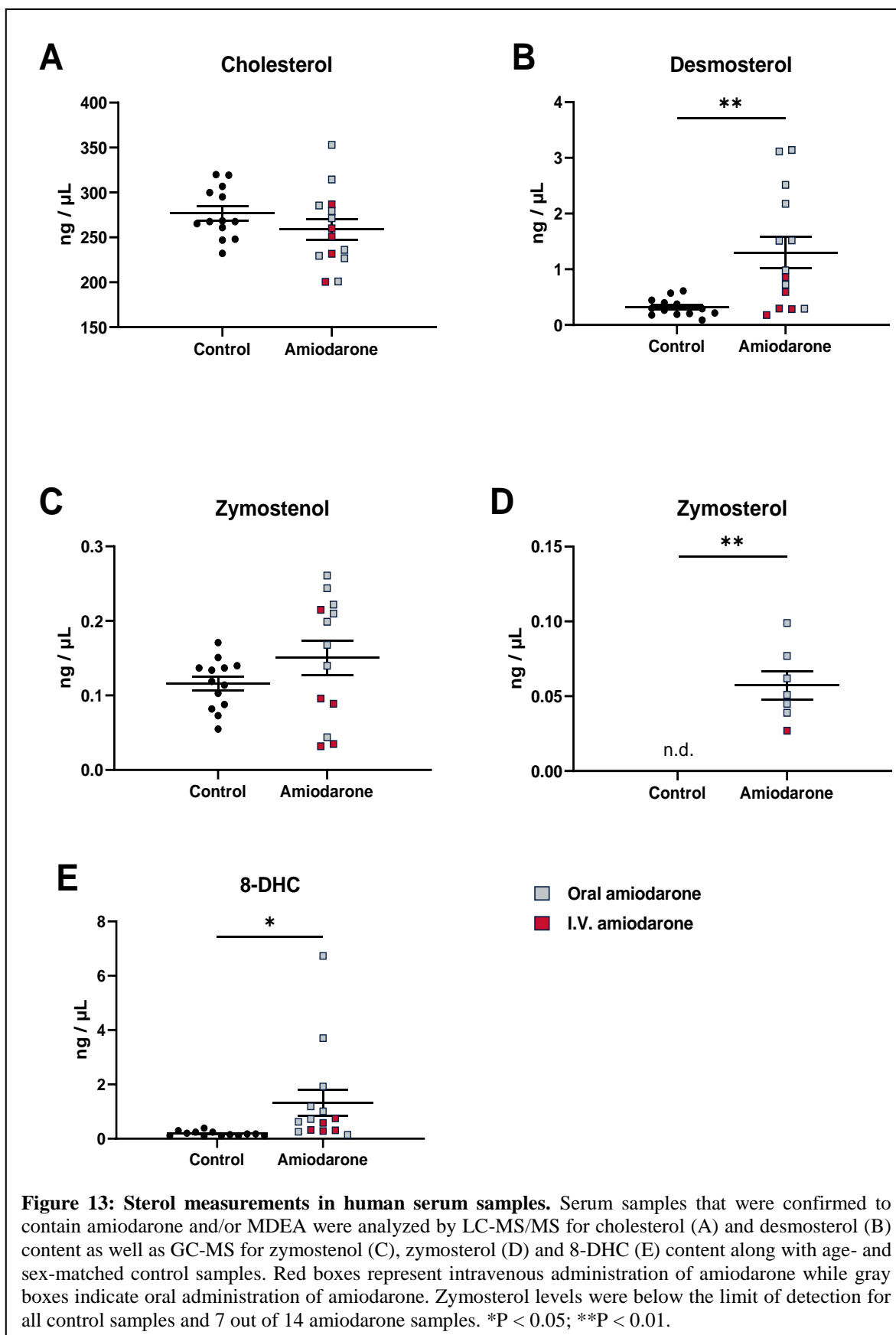


Figure 12: Amiodarone and MDEA are present in patient serum. Typical chromatograms and structures for amiodarone (A), MDEA (B) and the internal standard d₈-Aripiprazole (C). Amiodarone and MDEA were present in measurable quantities in 14 samples (D and E) that had amiodarone listed in their medical records. Red boxes indicate intravenous amiodarone administration while gray boxes indicate oral administration.



CHAPTER 4: DISCUSSION

Role of desmosterol in neuronal development

The outcome of our studies can be summarized as follows: A) cholesterol deficiency leads to early postnatal death or stillborn pups. B) Desmosterol is the second most abundant sterol at P0 during normal development, with a declining trajectory during development in to adulthood. C) In *Dhcr24*-KO mice, while desmosterol and 7-DHC are significantly elevated, cholesterol is greatly decreased. D) Greatly elevated desmosterol in Het brain at P0 continues to stay elevated in the adult brain. E) Changes in brain sterol composition lead to altered transcriptome response, affecting synaptic, lipid and nuclear receptor transcripts in a complex fashion. F) Total arborization of cultured *Dhcr24*-KO neurons is increased compared to WT neurons.

Studies in the SLOS mouse models were informative and provided a new insight into the human disorder [97-100], as the sterol biosynthesis pathway is conserved across the two species. SLOS is the most frequent human disorder caused by mutation in cholesterol biosynthesis enzymes, and SLOS transgenic mouse models recapitulate molecular and biochemical changes seen in SLOS patients [17, 42, 72, 101, 102]. Similarly, DHCR24 mutations in desmosterolosis patients share the same fundamental phenotype with the *Dhcr24*-KO mice – they have highly elevated desmosterol, and diminished levels of cholesterol. Thus, the highly conserved cholesterol biosynthesis pathways, and similarity of biochemical profile between human patients and transgenic mouse models suggest that the current model is a clinically relevant representation of pathophysiological processes that take place in the brain of human desmosterolosis patients.

While whole body cholesterol biosynthesis and metabolism have been extensively studied in the context of energy metabolism and cardiovascular diseases, the origin, role, metabolism and regulation of the CNS cholesterol pool remains understudied. As shown in this study, desmosterol is the second most abundant sterol in the brain with rapidly increasing levels prenatally, and steady levels in adulthood. Thus, this raises the interesting question: does desmosterol have a function of

its own, and can it influence normal brain function? Jansen et al. proposed that transient accumulation of desmosterol during early postnatal period may serve to increase the sterol pool in the brain [103]. This could be accomplished through different mechanisms due to the distinct chemical properties of desmosterol. Desmosterol has decreased propensity to be esterified as compared to cholesterol. Additionally, it cannot be hydroxylated to generate 24S-hydroxycholesterol and it is capable of activating the LXR-dependent pathway [103]. Based on the effects of desmosterol on neuronal arborization and synaptic plasticity transcripts that we have observed, it is conceivable that desmosterol may have additional roles in the regulation of neuronal differentiation and synaptic remodeling and this should be further investigated.

Our studies and previous findings raise an interesting question. In recessive diseases, heterozygous parents are typically asymptomatic, with the disease phenotype being expressed only in the offspring homozygous or compound heterozygous for the mutations. This might not be true in the case of *DHCR24* mutations. Namely, in the three clinical reports of desmosterolosis [20, 22, 26] in addition to description of affected individual, the authors assessed desmosterol levels in parents (carriers of *DHCR24* mutations). All six carriers had elevated plasma desmosterol levels compared to control samples. In addition, the cultured immortalized lymphocytes obtained from patient parents showed a 10-fold increase in desmosterol levels compared to control samples. This finding has potential clinical implications, raising a host of questions. At what level do sterol intermediates levels become detrimental? How wide is the “normal” range for cholesterol biosynthesis intermediates? Is the elevated level of desmosterol predisposing, protective or a modifying factor for another condition?

An interesting and important observation of our study is related to the significantly increased desmosterol levels of the *Dhcr24*-Het mice throughout their lifespan. With decreased *DHCR24* activity observed in the *Dhcr24*-Het mice, we speculate that 7-dehydrodesmosterol (7-DHD), the immediate precursor to desmosterol, would also be increased in the brain. This would

not be surprising and can be extrapolated from the increased 7-DHC levels in the *Dhcr24*-Het brains at P0 (**Figure 5**). The increase in 7-DHC suggests that intermediates upstream to desmosterol on the pathway would also be affected. Since both 7-DHC and 7-DHD are more prone to oxidation due to their chemical structure [104, 105], the resulting oxidative products may have cytotoxic effects in the brain. Thus, in the *DHCR24*^{+/-} heterozygous human population the elevated desmosterol and 7-DHD levels have the potential to result in elevated levels of oxysterols and increased oxidative stress, which might have a long-term effect on overall health status. These potential oxidative stress effects are likely to be regional and tissue-dependent, as we observed differences in desmosterol accumulation between the various brain regions. Thus, we propose that health status of the human heterozygous *DHCR24*^{+/-} carriers should be carefully assessed, as this single-copy mutation might affect more than one domain of health and lead to a predisposition to various disorders in which oxidative stress plays a pathophysiological part.

While desmosterol is greatly elevated in *Dhcr24*-KO and significantly decreased in *Dhcr7*-KO mice as compared to WT, 7-DHC was increased in both of these two mouse models, and both disorders are characterized by markedly decreased cholesterol levels in the brain. Thus, it is perhaps not surprising that the molecular and microanatomical changes also show some similarities between *Dhcr24*-KO and *Dhcr7*-KO mice. Namely, the affected gene expression, while not identical across the two mouse models, impact the same transcriptional networks, and increased neuronal arborization is a feature of both models. Untangling the precise origin of all these changes is challenging and we propose that the primary driver of the majority of common changes is lack of cholesterol, while the *Dhcr24*-KO specific changes are due to elevated desmosterol levels. However, we acknowledge that increased neural arborization can be potentially a result of increased 7-DHC observed in both models, and might be due to the previously reported toxic effect of 7-DHC derived oxysterols [91, 96].

In conclusion, desmosterol is an abundant, temporally regulated precursor of cholesterol in brain cells, with putative physiological function. Its disturbances might be a significant contributor to disease states, and this should be further investigated.

Amiodarone affects cholesterol biosynthesis

Our results can be summarized as follows: (A) Amiodarone inhibits Ebp in astrocytes and neurons leading to dose-dependent increases in zymosterol and zymostenol. (B) Genetic inhibition and chemical inhibition of Ebp yield similar results in Neuro2a cells. (C) Amiodarone and MDEA are present in measurable quantities in patient serum samples. (D) Patient samples with detectable levels of amiodarone or MDEA have elevated levels of desmosterol, 8-DHC and zymosterol as well as a slight increase in zymostenol.

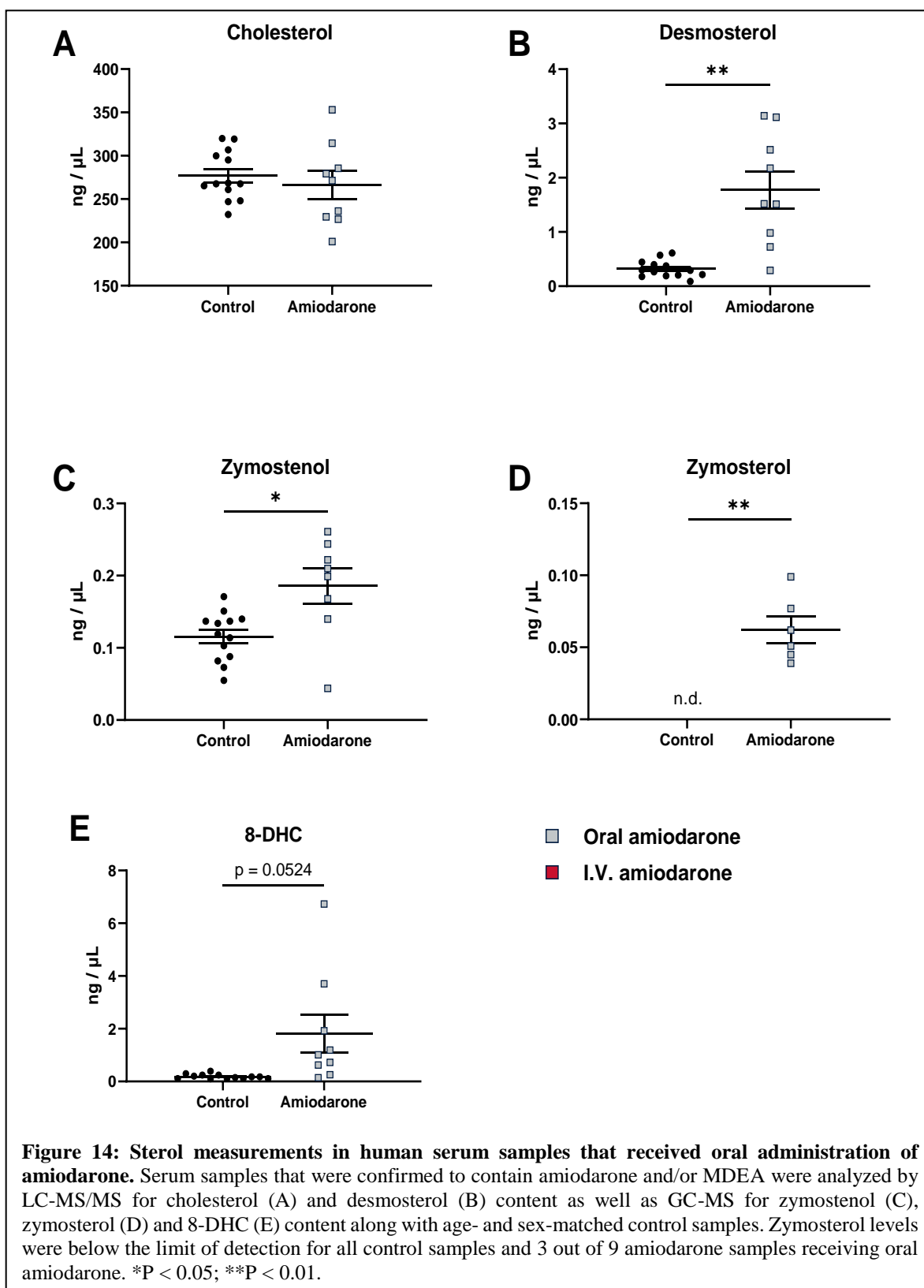
The biochemical findings from cell culture systems and patient serum implicate two enzymes that are subject to inhibition by amiodarone: Dhcr24 and Ebp. The strongest effect in neuronal cells is the inhibition of Ebp. Ebp is responsible for the conversion of zymosterol to 24-dehydrolathosterol and zymostenol to lathosterol, as well as the isomerization of 7-DHC to 8-DHC, thus explaining the elevation of zymostenol and zymosterol in the neuronal and astrocytic cultures in response to amiodarone treatment. The elegant studies by Moebius and colleagues [106-109] analyzed the pharmacological properties of EBP. In their work they found that, *in vitro*, EBP can bind structurally diverse drugs with high affinity, including amiodarone.

Interestingly, the increase in zymostenol due to amiodarone treatment in astrocytes is roughly 5 times higher than in neurons. Additionally, the magnitude of change in zymosterol is about twice as large in astrocytes as well, which may indicate that they are more susceptible to chemical alterations in cholesterol biosynthesis. Overall the profile in astrocytes and neurons was very similar to what was observed in *Ebp*-deficient cells.

Amiodarone measurements in the clinical population are in agreement with the study in cell culture system, suggesting an effect on more than one enzyme. An interesting trend appeared

in the desmosterol, zymostenol and zymosterol results when the administration method was taken into consideration. Intravenous administration (**Figure 13**, red boxes) tended to cluster with lower levels of the intermediates while oral administration in the form of a tablet (**Figure 13**, gray boxes) clustered at the higher end of the mentioned sterols. Interestingly, only 1 of the 5 samples with intravenous administration had detectable levels of zymosterol whereas it was detectable in 6 of 9 samples that received oral administration. In fact, when comparing only samples that had a history of oral amiodarone usage, the elevation in zymostenol becomes statistically significant, as well as increasing the mean desmosterol levels (**Figure 14**). It is important to take into consideration that amiodarone treatment can range from weeks to years [84]. Unfortunately, the length of treatment was not available for these samples, but intravenous administration is primarily used for short-term management of serious arrhythmias so it follows that those samples would have lesser effects reflected in their serum sterol levels. Thus, the alteration in sterol levels is apparently time-dependent which is consistent with the major risk factor for developing toxic neurological effects being treatment duration.

Amiodarone has a very narrow therapeutic range (1.0-2.5 $\mu\text{g/mL}$) [110] and the toxicity is linked to concentrations above 2.5 $\mu\text{g/mL}$ [111]. However, the highest level of amiodarone in the patient samples we analyzed was 0.176 $\mu\text{g/mL}$, while the remainder of the samples had a range of 0.0013 – 0.0184 $\mu\text{g/mL}$ (median 0.0061 $\mu\text{g/mL}$) (**Figure 12**). Despite the samples analyzed in the present study being much below the reported therapeutic range, let alone near the toxicity threshold, observable changes in cholesterol intermediates are still present and significant. These changes would be much more pronounced in amiodarone users with high plasma concentration of amiodarone. Furthermore, due to the lipophilic nature of amiodarone and MDEA it is likely that the tissue specific concentrations of these drugs is even higher than what is observed in the serum and thus the effects on cholesterol biosynthesis may be even more pronounced in tissue due to the local concentration of the drug.



While amiodarone has been beneficial in the treatment of life-threatening arrhythmias, it has many side effects. At the cellular/molecular levels, since amiodarone is lipophilic, it easily accumulates in cells where it can cause mitochondrial damage and structural and functional disturbances in the late endosomes and lysosomes. This may lead to a so-called ‘lipid traffic jam’ and in the liver, amiodarone use can lead to nonalcoholic steatohepatitis. Desmosterol levels in the liver and serum correlate with the severity of steatosis and inflammation [112]. The number of amiodarone prescriptions in the USA for 2006-2016 was 37,806,878 with a yearly average of 3,436,989 (median 3,404,961) [79]. Additionally, amiodarone is considered a category D drug by the FDA, meaning that there is positive evidence of human fetal risk and careful consideration is critical for the use of this drug during pregnancy. Therefore, careful clinical evaluation and monitoring of the adverse side effects is warranted in long-term amiodarone use.

This study provides insight into the consequences of amiodarone’s inhibition of cholesterol synthesis and warrants careful monitoring of blood biochemistry in amiodarone users. It is imperative that this monitoring goes beyond the standard cholesterol measurements as cholesterol levels on their own may not indicate a problem as seen in **Figure 13** and **Figure 14**, as there was no observable difference in cholesterol between the two groups but the levels of the intermediates differed greatly. Additionally, the screening of novel compounds with structures similar to amiodarone should include testing for the inhibition of the EBP and other sterol enzymes to avoid unintended interference with cholesterol biosynthesis.

Numerous studies have attempted to determine if plasma lipid measurements or pharmaceutical manipulations affect cognitive functions and brain neurochemistry [113, 114]. While there is no definitive answer when analyzing cholesterol levels in human serum samples, based on our limited studies in transgenic mouse models of cholesterol disorders, it is clear that serum sterol levels reflect cholesterol biosynthesis in brain and other tissues (**Figure 7**). However, the magnitude of change is much more pronounced in tissues compared to serum and the brain has

much larger change than other organs. Similarly, the levels of intermediates are much more representative of the defect in cholesterol synthesis than the level of cholesterol due in part to the effect of diet on cholesterol levels.

Conclusions

The characterization of desmosterolosis revealed a number of commonalities with what has been previously observed in various SLOS models. These include a drastic reduction in the amount of cholesterol present in the brain, prenatal lethality in knockouts, a marked alteration in sterol intermediate levels which result in alterations in gene transcription (**Table 1**) as well as the phenotype of primary neurons. It is important to keep in mind that these intermediates have other biological roles in addition to simply being just stepping stones on the way to cholesterol. However, a buildup of 7-DHC and desmosterol are not equal – due to the highly reactive nature of 7-DHC and its propensity to form oxidized sterols, known as oxysterols, 7-DHC buildup is particularly problematic as it has been shown that high levels of oxysterols are toxic [91]. It is important to consider the role that a desmosterol precursor, 7-dehydrodesmosterol, has been calculated to be equally as prone to oxidation as 7-DHC [104], however due to the reactive nature and relative scarcity of this sterol in tissues it was not measured in the present study.

In addition to genetic elevation of cholesterol intermediates there are significant number of medications that have elevation of cholesterol intermediates as a side effect. Previous screening studies estimate about 5% of compounds out of ~3,000 analyzed have unintended effects on cholesterol biosynthesis. It is obvious that more potent inhibitors of sterol enzymes are problematic, such was the case in the removal of triparanol from the market. Many of the side effects of triparanol that lead to its withdrawal from the market are analogous to what is observed in the side effects of amiodarone use. For example, triparanol induced cataracts whereas corneal microdeposits are observed in “virtually all patients who receive amiodarone for more than 6 months” [115].

The major focus in the present study was on the neurodevelopmental consequences of perturbed cholesterol biosynthesis. Altered levels of cholesterol and its replacement with intermediates has devastating effects on the development of the nervous system. Similarly the use of medications that disrupt cholesterol synthesis during pregnancy have significant negative effects on the developing fetus as seen in the case of amiodarone use during pregnancy [76] in addition to the well-described teratogenic effects of other cholesterol disrupting medications [63]. These disruptions are much more serious for developing neurons as their rate of cholesterol biosynthesis is much higher than that of mature neurons [9] so they will more quickly feel the effects of the disruption, which then translates to neurological and developmental issues in humans.

Future studies should focus on further exploring the extent to which unintended perturbations of cholesterol biosynthesis may contribute to side effects of commonly prescribed medications. Utilizing different models to understand the implications of these disruptions is vital in understanding the biological consequences that arise from disrupting cholesterol biosynthesis. Despite the fact that desmosterolosis is an incredibly rare disease, studying the etiology and pathophysiology of the disease illustrates the role certain biomolecules have in normal development. Likewise, understanding how different medications interact with this pathway may be informed by studying genetic disorders in the pathway and how they manifest. Furthermore, in the age of personalized medicine, understanding the full array of effects of a given medication is especially important when certain medications can interact and have devastating outcomes with different genotypes. For example, approximately 1.5% of the population carries a mutation in the *Dhcr7* gene that encodes 7-dehydrocholesterol reductase, the enzyme in which dysfunction leads to SLOS. These mutations have been shown to interact with either aripiprazole [70] or cariprazine [116], two commonly prescribed antipsychotics known to inhibit *DHCR7*, which can lead to devastating neurodevelopmental outcome in the event that a carrier of one of these mutations takes these drugs during pregnancy. Therefore, further study of disruptions in cholesterol biosynthesis

will not only help inform clinicians of potentially devastating side effects, but also expand on the current knowledge of a pathway that, while essential for life, is not fully understood.

APPENDIX A: STEROL INFORMATION

Table 2: Common names of sterols used with detailed information.

Common name	IUPAC name	CAS number	Molecular Formula	Other names
Cholesterol	(3 β)-cholest-5-en-3-ol	57-88-5	C ₂₇ H ₄₆ O	
Desmosterol	(3 β)-cholesta-5,24-dien-3-ol	313-04-2	C ₂₇ H ₄₄ O	24-Dehydrocholesterol
8-Dehydrocholesterol	(3 β)-Cholesta-5,8-dien-3-ol	70741-38-7	C ₂₇ H ₄₄ O	
7-Dehydrocholesterol	3 β -Cholesta-5,7-dien-3-ol	434-16-2	C ₂₇ H ₄₄ O	3 β -Hydroxy-5,7-cholestadiene; Provitamin D3
Lathosterol	(3 β ,5 α)-Cholest-7-en-3-ol	80-99-9	C ₂₇ H ₄₆ O	Δ 7-Cholestenol; γ -Cholestenol
Zymosterol	(3 β ,5 α)-Cholesta-8,24-dien-3-ol	128-33-6	C ₂₇ H ₄₄ O	8,24(5 α)-Cholestadien-3 β -ol
Zymostenol	(3 β ,5 α)-Cholest-8-en-3-ol	566-97-2	C ₂₇ H ₄₆ O	Δ ⁸ -Cholesterol
Lanosterol	(3 β)-Lanosta-8,24-dien-3-ol	79-63-0	C ₃₀ H ₅₀ O	8,24-Lanostadien-3 β -ol; 3 β -hydroxy-8,24-Lanostadiene

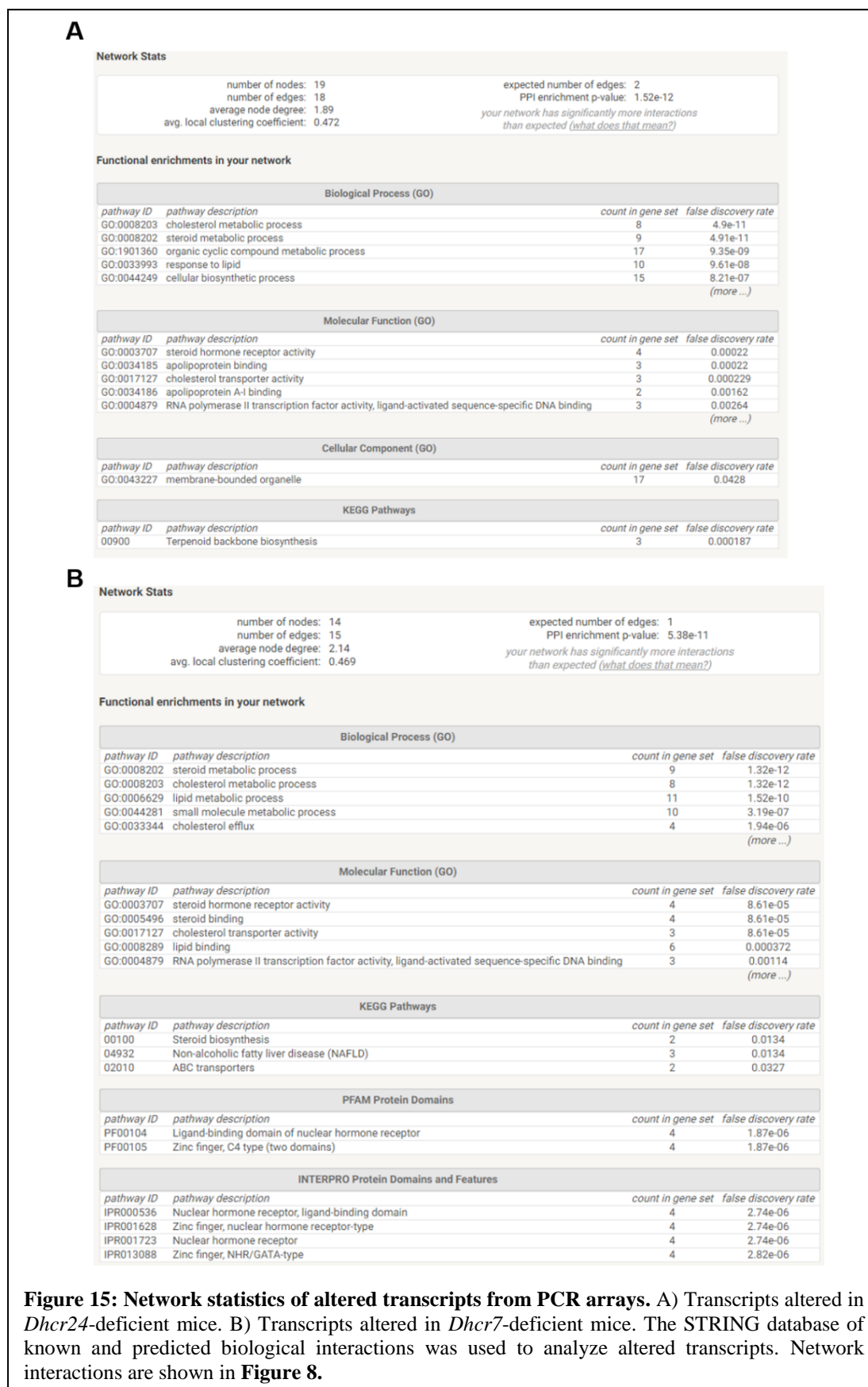
APPENDIX B: STEROL BIOSYNTHESIS DISORDERS

Table 3: Comparison of cholesterol synthesis disorders.

	SLOS	Desmosterolosis	Lathosterolosis	CDPX2
Gene	DHCR7	DHCR24	SC5D	EBP
Chromosome	11q13.4	1p32.3	11q23.3-q24.1	Xp11.23
Inheritance	Autosomal recessive	Autosomal recessive	Autosomal recessive	X-linked
Protein	475 aa 54489 Da	516 aa 60101 Da	299 aa 35301 Da	230 aa 26353 Da
Mutations identified	>200	8	6	57
Protein function	Reductase	Reductase	Reductase	Isomerase
Enzyme	EC1.3.1.21	EC1.3.1.72	EC1.14.19.20	EC5.3.3.5
Biochemical findings	↑ 7-DHC ↑ 8-DHC ↓ Desmosterol	↑ Desmosterol	↑ Lathosterol	↑ 8-DHC ↑ Zymostenol

Nomenclature Committee of the International Union of Biochemistry and Molecular Biology (IUBMB) describes each type of characterized enzyme for which an EC (Enzyme Commission) number has been provided.

APPENDIX C: NETWORK STATISTICS OF ALTERED TRANSCRIPTS FROM PCR ARRAYS



APPENDIX D: ZYMOSTEROL AND ZYMOSTENOL GC-MS CHROMATOGRAMS AND MASS SPECTRA

Zymosterol

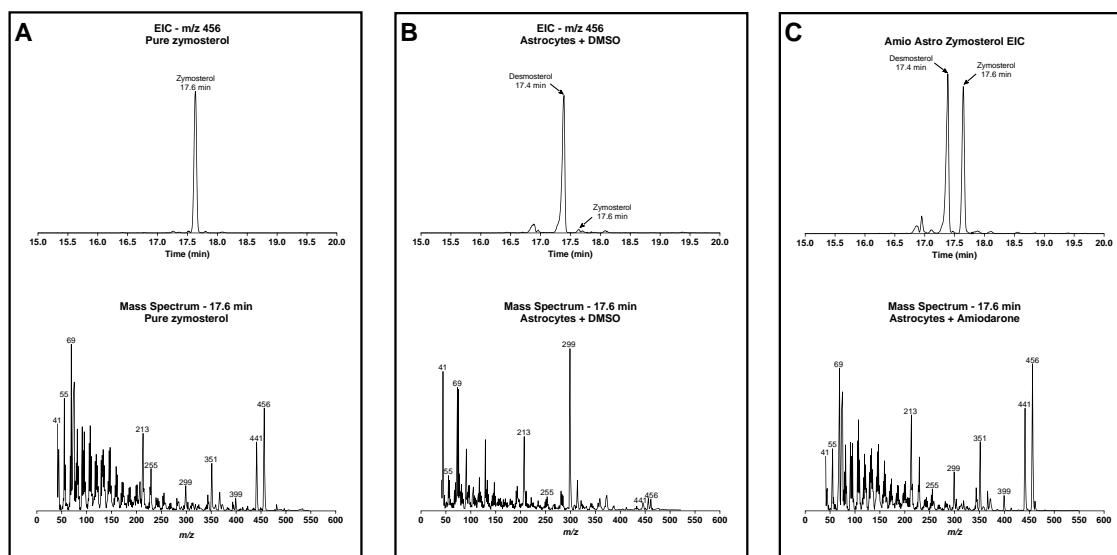


Figure 16: GC-MS analysis of zymosterol. A) Chromatogram (top) and mass spectrum (bottom) for pure zymosterol purchased from Kerfast. B) Typical chromatogram and mass spectrum obtained from control treated astrocytes. C) Typical chromatogram and mass spectrum obtained from astrocytes treated with 1 μ M amiodarone for 5 days. Note the increase in peak size in C as well as the increase in the m/z 456 ion upon treatment with amiodarone.

Zymostenol

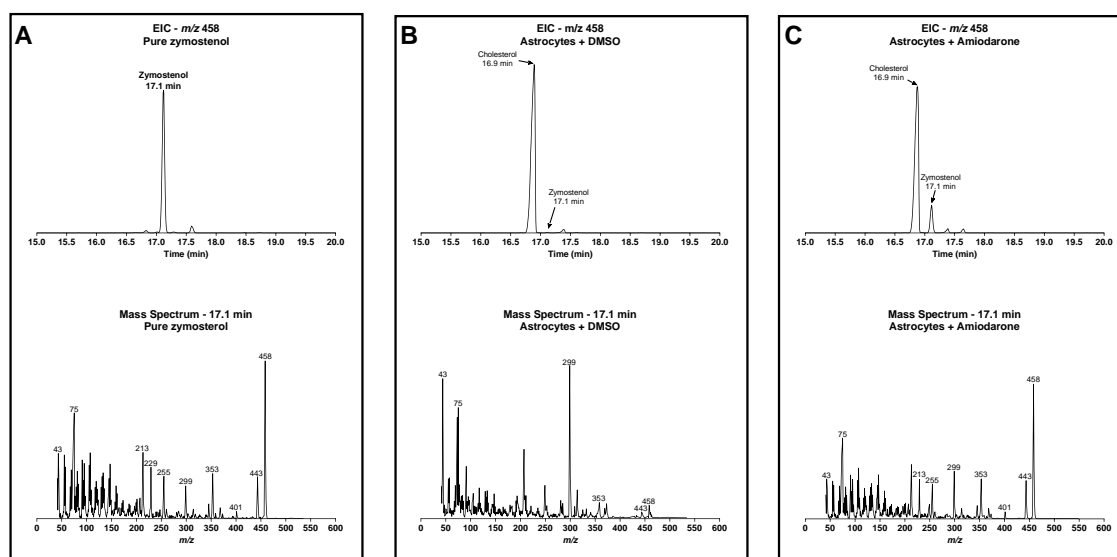


Figure 17: GC-MS analysis of zymostenol. A) Chromatogram (top) and mass spectrum (bottom) for pure zymostenol purchased from Kerfast. B) Typical chromatogram and mass spectrum obtained from control treated astrocytes. C) Typical chromatogram and mass spectrum obtained from astrocytes treated with 1 μ M amiodarone for 5 days. Note the increase in peak size in C as well as the increase in the m/z 458 ion upon treatment with amiodarone.

APPENDIX E: REAGENT TABLE

Reagent	Company	Catalog #
B-27 Supplement	Fisher	17504-044
D ₇ -Chol	Kerafast	EVU122
D ₇ -7-DHC	Kerafast	EVU123
D ₇ -8-DHC	Kerafast	EVU125
¹³ C-desmosterol	Kerafast	EVU127
¹³ C-lanosterol	Kerafast	EVU135
Rabbit α -DHCR24	Cell Signaling	2033S
Rabbit α -GAPDH	Cell Signaling	5174S
Mouse α - β -Actin	Cell Signaling	3700S
Rabbit α -MAP2	Cell Signaling	8707S
Radiance substrate	Azure	76318-638
Zymosterol	Avanti Polar Lipids	700068P-1mg
Zymostenol	Kerafast	EVU130
D ₈ -Aripiprazole	Sigma Aldrich	A-081-ML
Amiodarone	Sigma Aldrich	A8423-1G
PTAD	Sigma Aldrich	280992-5G
DHCR24 mice	Jackson Laboratory	12564
DHCR7 mice	Jackson Laboratory	007453
N2 supplement	Thermo Fisher	17502048
Hoechst dye	Thermo Fisher	H3570
BSTFA	Sigma Aldrich	T6381-10AMP
Goat α -mouse HRP	Sigma Aldrich	A9917-1ML
Goat α -rabbit HRP	Cell Signaling	7074S
HBSS w/o Ca ²⁺ , Mg ²⁺	VWR International	82024-308
TRIzol	Thermo Fisher	15596026
Igepal	Sigma Aldrich	I8896-100
RNeasy Mini Kit	Qiagen	74104
RNase-Free Dnase	Qiagen	79254
Extract-N-Amp PCR Ready Mix	Sigma Aldrich	E3004-1.2ML

BIBLIOGRAPHY

1. Jurevics, H. and P. Morell, *Cholesterol for synthesis of myelin is made locally, not imported into brain*. J Neurochem, 1995. **64**(2): p. 895-901.
2. Lutjohann, D. and K. von Bergmann, *24S-hydroxycholesterol: a marker of brain cholesterol metabolism*. Pharmacopsychiatry, 2003. **36 Suppl 2**: p. S102-6.
3. Pfrieger, F.W., *Outsourcing in the brain: do neurons depend on cholesterol delivery by astrocytes?* Bioessays, 2003. **25**(1): p. 72-8.
4. Strandberg, T.E. and R.S. Tilvis, *Physiological and pharmacological regulation of small intestinal cholesterol synthesis*. Gen Pharmacol, 1988. **19**(3): p. 321-9.
5. Shepherd, J., *Lipoprotein metabolism. An overview*. Drugs, 1994. **47 Suppl 2**: p. 1-10.
6. Dietschy, J.M. and S.D. Turley, *Cholesterol metabolism in the brain*. Curr Opin Lipidol, 2001. **12**(2): p. 105-12.
7. Tint, G.S., et al., *Defective cholesterol biosynthesis associated with the Smith-Lemli-Opitz syndrome*. N Engl J Med, 1994. **330**(2): p. 107-13.
8. Tint, G.S., et al., *Markedly increased tissue concentrations of 7-dehydrocholesterol combined with low levels of cholesterol are characteristic of the Smith-Lemli-Opitz syndrome*. J Lipid Res, 1995. **36**(1): p. 89-95.
9. Dietschy, J.M. and S.D. Turley, *Thematic review series: brain Lipids. Cholesterol metabolism in the central nervous system during early development and in the mature animal*. J Lipid Res, 2004. **45**(8): p. 1375-97.
10. Herman, G.E., *Disorders of cholesterol biosynthesis: prototypic metabolic malformation syndromes*. Hum Mol Genet, 2003. **12 Spec No 1**: p. R75-88.
11. Nicholas, H.J. and B.E. Thomas, *Cholesterol metabolism and the blood-brain barrier: an experimental study with 2-C14-sodium acetate*. Brain, 1961. **84**: p. 320-8.
12. Korade, Z., et al., *Expression and p75 neurotrophin receptor dependence of cholesterol synthetic enzymes in adult mouse brain*. Neurobiol Aging, 2007. **28**(10): p. 1522-31.
13. Korade, Z. and A.K. Kenworthy, *Lipid rafts, cholesterol, and the brain*. Neuropharmacology, 2008. **55**(8): p. 1265-73.
14. Cooper, M.K., et al., *A defective response to Hedgehog signaling in disorders of cholesterol biosynthesis*. Nat Genet, 2003. **33**(4): p. 508-13.
15. Huang, T.L. and J.F. Chen, *Cholesterol and lipids in depression: stress, hypothalamo-pituitary-adrenocortical axis, and inflammation/immunity*. Adv Clin Chem, 2005. **39**: p. 81-105.
16. You, H., et al., *The relationship between statins and depression: a review of the literature*. Expert Opin Pharmacother, 2013. **14**(11): p. 1467-76.
17. Porter, F.D., *Smith-Lemli-Opitz syndrome: pathogenesis, diagnosis and management*. Eur J Hum Genet, 2008. **16**(5): p. 535-41.
18. Steiner, R.D., et al., *Sterol balance in the Smith-Lemli-Opitz syndrome. Reduction in whole body cholesterol synthesis and normal bile acid production*. J Lipid Res, 2000. **41**(9): p. 1437-47.

19. Allen, L.B., et al., *Desmosterolosis and desmosterol homeostasis in the developing mouse brain*. J Inherit Metab Dis, 2019. **42**(5): p. 934-943.
20. Andersson, H.C., L. Kratz, and R. Kelley, *Desmosterolosis presenting with multiple congenital anomalies and profound developmental delay*. Am J Med Genet, 2002. **113**(4): p. 315-9.
21. Dias, C., et al., *Desmosterolosis: an illustration of diagnostic ambiguity of cholesterol synthesis disorders*. Orphanet J Rare Dis, 2014. **9**: p. 94.
22. FitzPatrick, D.R., et al., *Clinical phenotype of desmosterolosis*. Am J Med Genet, 1998. **75**(2): p. 145-52.
23. Rohanizadegan, M. and S. Sacharow, *Desmosterolosis presenting with multiple congenital anomalies*. Eur J Med Genet, 2018. **61**(3): p. 152-156.
24. Schaaf, C.P., et al., *Desmosterolosis-phenotypic and molecular characterization of a third case and review of the literature*. Am J Med Genet A, 2011. **155A**(7): p. 1597-604.
25. Waterham, H.R., et al., *Mutations in the 3beta-hydroxysterol Delta24-reductase gene cause desmosterolosis, an autosomal recessive disorder of cholesterol biosynthesis*. Am J Hum Genet, 2001. **69**(4): p. 685-94.
26. Zolotushko, J., et al., *The desmosterolosis phenotype: spasticity, microcephaly and micrognathia with agenesis of corpus callosum and loss of white matter*. Eur J Hum Genet, 2011. **19**(9): p. 942-6.
27. Rosenbaum, A.I. and F.R. Maxfield, *Niemann-Pick type C disease: molecular mechanisms and potential therapeutic approaches*. J Neurochem, 2011. **116**(5): p. 789-95.
28. Kolsch, H., et al., *CYP46A1 variants influence Alzheimer's disease risk and brain cholesterol metabolism*. Eur Psychiatry, 2009. **24**(3): p. 183-90.
29. Leoni, V. and C. Caccia, *Study of cholesterol metabolism in Huntington's disease*. Biochem Biophys Res Commun, 2014. **446**(3): p. 697-701.
30. Leoni, V. and C. Caccia, *The impairment of cholesterol metabolism in Huntington disease*. Biochim Biophys Acta, 2015. **1851**(8): p. 1095-105.
31. Martin, M.G., F. Pfrieger, and C.G. Dotti, *Cholesterol in brain disease: sometimes determinant and frequently implicated*. EMBO Rep, 2014. **15**(10): p. 1036-52.
32. Sparks, D.L., *Cholesterol metabolism and brain amyloidosis: evidence for a role of copper in the clearance of Abeta through the liver*. Curr Alzheimer Res, 2007. **4**(2): p. 165-9.
33. Bianconi, S.E., et al., *Pathogenesis, Epidemiology, Diagnosis and Clinical Aspects of Smith-Lemli-Opitz Syndrome*. Expert Opin Orphan Drugs, 2015. **3**(3): p. 267-280.
34. Chang, S., et al., *Elevated Autophagy and Mitochondrial Dysfunction in the Smith-Lemli-Opitz Syndrome*. Mol Genet Metab Rep, 2014. **1**: p. 431-442.
35. Herman, G.E. and L. Kratz, *Disorders of sterol synthesis: beyond Smith-Lemli-Opitz syndrome*. Am J Med Genet C Semin Med Genet, 2012. **160C**(4): p. 301-21.
36. Kelley, R.I., *Inborn errors of cholesterol biosynthesis*. Adv Pediatr, 2000. **47**: p. 1-53.
37. Nwokoro, N.A., C.A. Wassif, and F.D. Porter, *Genetic disorders of cholesterol biosynthesis in mice and humans*. Mol Genet Metab, 2001. **74**(1-2): p. 105-19.
38. Moebius, F.F., et al., *Molecular cloning and expression of the human delta7-sterol reductase*. Proc Natl Acad Sci U S A, 1998. **95**(4): p. 1899-902.

39. Battaile, K.P., et al., *Carrier frequency of the common mutation IVS8-1G>C in DHCR7 and estimate of the expected incidence of Smith-Lemli-Opitz syndrome*. Mol Genet Metab, 2001. **72**(1): p. 67-71.
40. Cross, J.L., et al., *Determination of the allelic frequency in Smith-Lemli-Opitz syndrome by analysis of massively parallel sequencing data sets*. Clin Genet, 2015. **87**(6): p. 570-5.
41. Ginat, S., et al., *Lowered DHCR7 activity measured by ergosterol conversion in multiple cell types in Smith-Lemli-Opitz syndrome*. Mol Genet Metab, 2004. **83**(1-2): p. 175-83.
42. Porter, F.D., *Malformation syndromes due to inborn errors of cholesterol synthesis*. J Clin Invest, 2002. **110**(6): p. 715-24.
43. Boland, M.R. and N.P. Tatonetti, *Investigation of 7-dehydrocholesterol reductase pathway to elucidate off-target prenatal effects of pharmaceuticals: a systematic review*. Pharmacogenomics J, 2016. **16**(5): p. 411-29.
44. Sikora, D.M., et al., *The near universal presence of autism spectrum disorders in children with Smith-Lemli-Opitz syndrome*. Am J Med Genet A, 2006. **140**(14): p. 1511-8.
45. Tierney, E., et al., *Abnormalities of cholesterol metabolism in autism spectrum disorders*. Am J Med Genet B Neuropsychiatr Genet, 2006. **141B**(6): p. 666-8.
46. Anderson, R., et al., *Lathosterolosis: A Relatively Mild Case with Cataracts and Learning Difficulties*. JIMD Rep, 2019. **44**: p. 79-84.
47. Derry, J.M., et al., *Mutations in a delta 8-delta 7 sterol isomerase in the tattered mouse and X-linked dominant chondrodysplasia punctata*. jderry@immunex.com. Nat Genet, 1999. **22**(3): p. 286-90.
48. Kelley, R.I., et al., *Abnormal sterol metabolism in patients with Conradi-Hunermann-Happle syndrome and sporadic lethal chondrodysplasia punctata*. Am J Med Genet, 1999. **83**(3): p. 213-9.
49. Uwechue, I.C., et al., *The mouse X-linked developmental mutant, tattered, lies between DXMit55 and Xkh and is associated with hyperkeratinization*. Genomics, 1996. **37**(2): p. 238-41.
50. Arnold, A.W., et al., *Conradi-Hunermann-Happle syndrome in males vs. MEND syndrome (male EBP disorder with neurological defects)*. Br J Dermatol, 2012. **166**(6): p. 1309-13.
51. Aughton, D.J., et al., *X-linked dominant chondrodysplasia punctata (CDPX2) caused by single gene mosaicism in a male*. Am J Med Genet A, 2003. **116A**(3): p. 255-60.
52. Sutphen, R., et al., *XXY male with X-linked dominant chondrodysplasia punctata (Happle syndrome)*. Am J Med Genet, 1995. **57**(3): p. 489-92.
53. Wechsler, A., et al., *Generation of viable cholesterol-free mice*. Science, 2003. **302**(5653): p. 2087.
54. Ohyama, Y., et al., *Studies on the transcriptional regulation of cholesterol 24-hydroxylase (CYP46A1): marked insensitivity toward different regulatory axes*. J Biol Chem, 2006. **281**(7): p. 3810-20.
55. Heverin, M., et al., *Studies on the cholesterol-free mouse: strong activation of LXR-regulated hepatic genes when replacing cholesterol with desmosterol*. Arterioscler Thromb Vasc Biol, 2007. **27**(10): p. 2191-7.

56. Lu, X., et al., *DHCR24-knockout embryonic fibroblasts are susceptible to serum withdrawal-induced apoptosis because of dysfunction of caveolae and insulin-Akt-Bad signaling*. *Endocrinology*, 2006. **147**(6): p. 3123-32.
57. Mirza, R., et al., *Increased expression of aquaporin-3 in the epidermis of DHCR24 knockout mice*. *Br J Dermatol*, 2008. **158**(4): p. 679-84.
58. Mirza, R., et al., *DHCR24 gene knockout mice demonstrate lethal dermatopathy with differentiation and maturation defects in the epidermis*. *J Invest Dermatol*, 2006. **126**(3): p. 638-47.
59. Mirza, R., et al., *Requirement of DHCR24 for postnatal development of epidermis and hair follicles in mice*. *Am J Dermatopathol*, 2009. **31**(5): p. 446-52.
60. Kuehnle, K., et al., *Prosurvival effect of DHCR24/Seladin-1 in acute and chronic responses to oxidative stress*. *Mol Cell Biol*, 2008. **28**(2): p. 539-50.
61. Steinberg, D., *The cholesterol wars : the skeptics vs. the preponderance of evidence*. 1st ed. 2007, San Diego, Calif.: Academic Press. xx, 227 p., 3 p. of plates.
62. Kirby, T.J., *Cataracts produced by triparanol. (MER-29)*. *Trans Am Ophthalmol Soc*, 1967. **65**: p. 494-543.
63. Roux, C., C. Horvath, and R. Dupuis, *Teratogenic action and embryo lethality of AY 9944R. Prevention by a hypercholesterolemia-provoking diet*. *Teratology*, 1979. **19**(1): p. 35-8.
64. Correa-Cerro, L.S., et al., *Development and characterization of a hypomorphic Smith-Lemli-Opitz syndrome mouse model and efficacy of simvastatin therapy*. *Hum Mol Genet*, 2006. **15**(6): p. 839-51.
65. Xu, L., et al., *7-Dehydrocholesterol-derived oxysterols and retinal degeneration in a rat model of Smith-Lemli-Opitz syndrome*. *Biochim Biophys Acta*, 2012. **1821**(6): p. 877-83.
66. Kim, H.Y., et al., *Inhibitors of 7-Dehydrocholesterol Reductase: Screening of a Collection of Pharmacologically Active Compounds in Neuro2a Cells*. *Chem Res Toxicol*, 2016. **29**(5): p. 892-900.
67. Korade, Z., et al., *The Effect of Small Molecules on Sterol Homeostasis: Measuring 7-Dehydrocholesterol in Dhcr7-Deficient Neuro2a Cells and Human Fibroblasts*. *J Med Chem*, 2016. **59**(3): p. 1102-15.
68. Wages, P.A., et al., *Identification and characterization of prescription drugs that change levels of 7-dehydrocholesterol and desmosterol*. *J Lipid Res*, 2018. **59**(10): p. 1916-1926.
69. Korade, Z., et al., *Effect of psychotropic drug treatment on sterol metabolism*. *Schizophr Res*, 2017. **187**: p. 74-81.
70. Genaro-Mattos, T.C., et al., *Maternal aripiprazole exposure interacts with 7-dehydrocholesterol reductase mutations and alters embryonic neurodevelopment*. *Mol Psychiatry*, 2019. **24**(4): p. 491-500.
71. Bulletins--Obstetrics, A.C.O.P., *ACOG Practice Bulletin: Clinical management guidelines for obstetrician-gynecologists number 92, April 2008 (replaces practice bulletin number 87, November 2007). Use of psychiatric medications during pregnancy and lactation*. *Obstet Gynecol*, 2008. **111**(4): p. 1001-20.
72. Porter, F.D. and G.E. Herman, *Malformation syndromes caused by disorders of cholesterol synthesis*. *J Lipid Res*, 2011. **52**(1): p. 6-34.

73. Pollak, P.T., A.D. Sharma, and S.G. Carruthers, *Elevation of serum total cholesterol and triglyceride levels during amiodarone therapy*. Am J Cardiol, 1988. **62**(9): p. 562-5.
74. Pollak, P.T. and M.H. Tan, *Elevation of high-density lipoprotein cholesterol in humans during long-term therapy with amiodarone*. Am J Cardiol, 1999. **83**(2): p. 296-300, A7.
75. Simonen, P., et al., *Desmosterol accumulation in users of amiodarone*. J Intern Med, 2018. **283**(1): p. 93-101.
76. Mikovic, Z., et al., *Developmental delay associated with normal thyroidal function and long-term amiodarone therapy during fetal and neonatal life*. Biomed Pharmacother, 2010. **64**(6): p. 396-8.
77. Amiodarone Hydrochloride [package insert]. Philadelphia, P., Wyeth Pharmaceuticals Inc. 2004.
78. Humphries, E.S. and C. Dart, *Neuronal and Cardiovascular Potassium Channels as Therapeutic Drug Targets: Promise and Pitfalls*. J Biomol Screen, 2015. **20**(9): p. 1055-73.
79. Kane, S. *Amiodarone Hydrochloride*. November 24, 2018 [cited 2019 October 24]; Available from: <https://clinicaltrials.gov/ct2/show/study/NCT01711111>.
80. World Health Organization Model List of Essential Medicines, 21st List, 2019. Geneva: World Health Organization 2019, (Licence: CC BY-NC-SA 3.0 IGO.).
81. January, C.T., et al., *2014 AHA/ACC/HRS guideline for the management of patients with atrial fibrillation: a report of the American College of Cardiology/American Heart Association Task Force on Practice Guidelines and the Heart Rhythm Society*. J Am Coll Cardiol, 2014. **64**(21): p. e1-76.
82. Fox, L.M., *The Science and Practice of Pharmacy, 21st Edition*. Am J Pharm Educ, 2006. **70**(3).
83. Pollak, P.T., A.D. Sharma, and S.G. Carruthers, *Correlation of amiodarone dosage, heart rate, QT interval and corneal microdeposits with serum amiodarone and desethylamiodarone concentrations*. Am J Cardiol, 1989. **64**(18): p. 1138-43.
84. Orr, C.F. and J.E. Ahlskog, *Frequency, characteristics, and risk factors for amiodarone neurotoxicity*. Arch Neurol, 2009. **66**(7): p. 865-9.
85. Mesens, N., et al., *Phospholipidosis in rats treated with amiodarone: serum biochemistry and whole genome micro-array analysis supporting the lipid traffic jam hypothesis and the subsequent rise of the biomarker BMP*. Toxicol Pathol, 2012. **40**(3): p. 491-503.
86. Levitan, I., et al., *Cholesterol and ion channels*. Subcell Biochem, 2010. **51**: p. 509-49.
87. Jirsova, K., et al., *Cold jet: a method to obtain pure Schwann cell cultures without the need for cytotoxic, apoptosis-inducing drug treatment*. J Neurosci Methods, 1997. **78**(1-2): p. 133-7.
88. Tint, G.S., et al., *The use of the Dhcr7 knockout mouse to accurately determine the origin of fetal sterols*. J Lipid Res, 2006. **47**(7): p. 1535-41.
89. Lamberson, C.R., et al., *Unusual kinetic isotope effects of deuterium reinforced polyunsaturated fatty acids in tocopherol-mediated free radical chain oxidations*. J Am Chem Soc, 2014. **136**(3): p. 838-41.
90. Korade, Z., A.K. Kenworthy, and K. Mirnics, *Molecular consequences of altered neuronal cholesterol biosynthesis*. J Neurosci Res, 2009. **87**(4): p. 866-75.

91. Korade, Z., et al., *Biological activities of 7-dehydrocholesterol-derived oxysterols: implications for Smith-Lemli-Opitz syndrome*. J Lipid Res, 2010. **51**(11): p. 3259-69.
92. Yang, C., et al., *Sterol intermediates from cholesterol biosynthetic pathway as liver X receptor ligands*. J Biol Chem, 2006. **281**(38): p. 27816-26.
93. Jiang, X.S., et al., *Quantitative proteomics analysis of inborn errors of cholesterol synthesis: identification of altered metabolic pathways in DHCR7 and SC5D deficiency*. Mol Cell Proteomics, 2010. **9**(7): p. 1461-75.
94. Xu, L., et al., *DHCEO accumulation is a critical mediator of pathophysiology in a Smith-Lemli-Opitz syndrome model*. Neurobiol Dis, 2012. **45**(3): p. 923-9.
95. Korade, Z., et al., *NR1F is a regulator of neuronal cholesterol biosynthesis genes*. J Mol Neurosci, 2009. **38**(2): p. 152-8.
96. Xu, L., et al., *An oxysterol biomarker for 7-dehydrocholesterol oxidation in cell/mouse models for Smith-Lemli-Opitz syndrome*. J Lipid Res, 2011. **52**(6): p. 1222-33.
97. Korade, Z., et al., *Antioxidant supplementation ameliorates molecular deficits in Smith-Lemli-Opitz syndrome*. Biol Psychiatry, 2014. **75**(3): p. 215-22.
98. Sharif, N.F., et al., *Oxidative stress, serotonergic changes and decreased ultrasonic vocalizations in a mouse model of Smith-Lemli-Opitz syndrome*. Genes Brain Behav, 2017. **16**(6): p. 619-626.
99. Sparks, S.E., et al., *Decreased cerebral spinal fluid neurotransmitter levels in Smith-Lemli-Opitz syndrome*. J Inher Metab Dis, 2014. **37**(3): p. 415-20.
100. Waage-Baudet, H., et al., *Abnormal serotonergic development in a mouse model for the Smith-Lemli-Opitz syndrome: implications for autism*. Int J Dev Neurosci, 2003. **21**(8): p. 451-9.
101. Porter, F.D., *RSH/Smith-Lemli-Opitz syndrome: a multiple congenital anomaly/mental retardation syndrome due to an inborn error of cholesterol biosynthesis*. Mol Genet Metab, 2000. **71**(1-2): p. 163-74.
102. Porter, F.D., *Human malformation syndromes due to inborn errors of cholesterol synthesis*. Curr Opin Pediatr, 2003. **15**(6): p. 607-13.
103. Jansen, M., et al., *What dictates the accumulation of desmosterol in the developing brain?* FASEB J, 2013. **27**(3): p. 865-70.
104. Lamberson, C.R., et al., *Propagation rate constants for the peroxidation of sterols on the biosynthetic pathway to cholesterol*. Chem Phys Lipids, 2017. **207**(Pt B): p. 51-58.
105. Yin, H., L. Xu, and N.A. Porter, *Free radical lipid peroxidation: mechanisms and analysis*. Chem Rev, 2011. **111**(10): p. 5944-72.
106. Moebius, F.F., et al., *Yeast sterol C8-C7 isomerase: identification and characterization of a high-affinity binding site for enzyme inhibitors*. Biochemistry, 1996. **35**(51): p. 16871-8.
107. Moebius, F.F., et al., *Cloning of an emopamil-binding protein (EBP)-like protein that lacks sterol delta8-delta7 isomerase activity*. Biochem J, 2003. **374**(Pt 1): p. 229-37.
108. Moebius, F.F., et al., *Pharmacological analysis of sterol delta8-delta7 isomerase proteins with [³H]ifenprodil*. Mol Pharmacol, 1998. **54**(3): p. 591-8.

109. Moebius, F.F., et al., *High affinity of sigma 1-binding sites for sterol isomerization inhibitors: evidence for a pharmacological relationship with the yeast sterol C8-C7 isomerase*. Br J Pharmacol, 1997. **121**(1): p. 1-6.
110. Rotmensch, H.H., et al., *Steady-state serum amiodarone concentrations: relationships with antiarrhythmic efficacy and toxicity*. Ann Intern Med, 1984. **101**(4): p. 462-9.
111. Haffajee, C.I., *Clinical pharmacokinetics of amiodarone*. Clin Cardiol, 1987. **10**(7 Suppl 1): p. I6-9.
112. Simonen, M., et al., *Desmosterol in human nonalcoholic steatohepatitis*. Hepatology, 2013. **58**(3): p. 976-82.
113. Cenik, B., et al., *Plasma sterols and depressive symptom severity in a population-based cohort*. PLoS One, 2017. **12**(9): p. e0184382.
114. Wellington, C.L. and R. Frikke-Schmidt, *Relation between plasma and brain lipids*. Curr Opin Lipidol, 2016. **27**(3): p. 225-32.
115. Dovie, J.M. and A.S. Gurwood, *Acute onset of halos and glare: bilateral corneal epithelial edema with cystic eruptions--atypical presentation of amiodarone keratopathy*. Optometry, 2006. **77**(2): p. 76-81.
116. Genaro-Mattos, T.C., et al., *Dichlorophenyl piperazines, including a recently-approved atypical antipsychotic, are potent inhibitors of DHCR7, the last enzyme in cholesterol biosynthesis*. Toxicol Appl Pharmacol, 2018. **349**: p. 21-28.